

# Single Chain Slip-Spring Model for Fast Rheology Simulations of Entangled Polymers on GPU

Takashi Uneyama\*

JST-CREST, Institute for Chemical Research, Kyoto University,  
Gokasho, Uji 611-0011, Japan

## Abstract

We propose a single chain slip-spring model, which is based on the slip-spring model by Likhtman [A. E. Likhtman, *Macromolecules*, **38**, 6128 (2005)], for fast rheology simulations of entangled polymers on a GPU. We modify the original slip-spring model slightly for efficient calculations on a GPU. Our model is designed to satisfy the detailed balance condition, which enables us to analyze its static or linear response properties easily. We theoretically analyze several statistical properties of the model, such as the linear response, which will be useful to analyze simulation data. We show that our model can reproduce several rheological properties such as the linear viscoelasticity or the viscosity growth qualitatively. We also show that the use of a GPU can improve the performance drastically.

**Keywords:** Slip-Spring, Entangled Polymer, Linear Response Theory, GPU

## 1 Introduction

Polymeric liquids exhibit various interesting macroscopic flows. To simulate macroscopic flow behaviors of entangled polymeric materials, we need to incorporate microscopic or mesoscopic polymer models (which reproduces required rheological properties) with the macroscopic fluid model (such as the Cauchy equation). Considering the computational costs, phenomenological constitutive equation models [1–4] are reasonable for macroscopic simulations. However, most of constitutive equation models involve rather rough or physically unclear approximations, which is not fully justified. To avoid such uncertainties, we can use microscopic or mesoscopic molecular models [5–12]. Although these molecular models also involve approximations, generally they require less phenomenological parameters, and we expect they are more precise than constitutive equation models. Thus we expect the use of molecular models instead of constitutive equation models can improve the macroscopic flow simulation.

Several different methods have been proposed to incorporate the mesoscopic polymer models with macroscopic fluid models. For example, the CONNFFESSIT type methods [13], the Lagrangian particle based methods [14, 15], or recently developed finite volume based hybrid method [16, 17] were proposed and achieved success to simulate macroscopic flows of polymers. Because these models directly combine different models which have different time and length scales (microscopic or mesoscopic rheological model, and macroscopic fluid model), we call them “multiscale” simulation models in this work. In these multiscale models, microscopic or mesoscopic rheological simulations are directly used to calculate macroscopic quantity such as the stress tensor, instead of phenomenological constitutive equation models. In other words, microscopic or mesoscopic simulations are embedded to macroscopic fluid elements. Clearly such simulations require many microscopic or mesoscopic rheological simulations which are numerically not efficient.

---

\*E-mail: uneyama@scl.kyoto-u.ac.jp, Tel: +81-774-38-3147, Fax: +81-774-38-3139

To simulate large scale and/or long time macroscopic phenomena, therefore it is demanding to perform many microscopic or mesoscopic simulations efficiently.

One possible way is to use hardware for acceleration. So far, several acceleration hardware (such as MDGRAPE [18–20], ClearSpeed [21, 22], or Cell Broadband Engine [23–25]) have been developed and utilized to accelerate calculations. Recently, the acceleration by a graphic processor unit (GPU) [26–30], which is called general purpose GPU (GPGPU) programming [31], is utilized to accelerate various calculations including molecular dynamics [32, 33], fluid dynamics [34], Monte Carlo models [35], or stochastic differential equation models [36]. It is reported that GPUs can accelerate simulations drastically, although the efficiency strongly depends on a target. Because GPUs are much cheaper than other acceleration hardware and new GPUs are developed continuously, they are considered to be promising compared with other previous acceleration hardware. Thus we expect that rheological simulations on a GPU will be a good candidate for the embedded fast rheological simulation.

In this work we employ the slip-spring model, which is originally proposed by Likhtman [10] to study the structure and dynamics of entangled polymers, for simulations on a GPU. We propose a slightly modified, single chain version of the slip-spring model. We design our model to be suitable for simulations on a GPU. We also design our model to fully satisfy the detailed balance condition. We derive several statistical properties such as equilibrium probability distributions or a formula for the relaxation modulus. By performing rheological simulations both on a CPU and on a GPU, we study rheological properties of the model and the acceleration effect by a GPU. It is shown that our model reproduces rheological properties reasonably and it enables efficient calculations on a GPU.

## 2 Model

Although there are various mesoscopic molecular models to calculate rheological properties of entangled polymers [5–12], not all models are suitable for simulations on a GPU. In this work, we employ the slip-spring model proposed by Likhtman [10]. In the Likhtman’s original slip-spring model, polymer chains are expressed as ideal non-interacting Rouse chains and the entanglement effect is mimicked by slip-springs. One end of a slip-spring is fixed in space and another end is attached to the polymer chain. As we will show later, such a model is suitable for calculations on a GPU.

In this section, we show a single chain slip-spring model, which is a variant of the original slip-spring model. We modify the Likhtman’s model slightly to make it suitable for simulations on a GPU. To implement simulation programs on a GPU, we need to use GPU specific programming environment and it has several limitations. Thus we design our dynamics model to be as simple as possible. At the same time, to make the model physically natural and to make static properties simple, we attempt to make the dynamics model to satisfy the detailed balance condition. We also discuss about the equilibrium statistical properties and the linear response theory of the slip-spring model, which is useful to calculate the linear viscoelasticity.

### 2.1 Free Energy, Grand Potential, and Equilibrium Statistics

We first describe the model of our single chain slip-spring model. We model an entangled polymer chain by an ideal Rouse chain and slip-springs. The conformation of a polymer chain is expressed by positions of beads  $\{\mathbf{R}_i\}$ , where  $i = 1, 2, \dots, N$  is the bead index ( $N$  is the total number of beads). The conformation of slip-springs are expressed by two set of variables; the bead indices of slip-spring  $\{S_j\}$  and the anchoring point positions  $\{\mathbf{A}_j\}$ , where  $j = 1, 2, \dots, Z$  with  $Z \geq 0$  being the total number of slip-springs. One end of the  $j$ -th slip-spring is attached to the  $S_j$ -th bead of a polymer chain, and another end is anchored in space, at  $\mathbf{A}_j$ . We assume that  $S_j$  is an integer value and  $1 \leq S_j \leq N$ . The total number of slip-springs  $Z$  is not constant because slip-springs can be spontaneously constructed or destructed. Thus variables  $\{\mathbf{R}_i\}$ ,  $\{\mathbf{A}_j\}$ ,  $\{S_j\}$ , and  $Z$  are required to specify a state uniquely.

To make the statistical mechanical properties of the model clearly, we first describe the free energy of a single chain with slip-springs. The free energy of a polymer chain and attached slip-springs can be expressed as follows.

$$\mathcal{F}(\{\mathbf{R}_i\}, \{\mathbf{A}_j\}, \{S_j\}, Z) = \sum_{i=1}^{N-1} \frac{3k_B T}{2b^2} (\mathbf{R}_{i+1} - \mathbf{R}_i)^2 + \sum_{j=1}^Z \frac{3k_B T}{2N_s b^2} (\mathbf{R}_{S_j} - \mathbf{A}_j)^2 \quad (1)$$

where  $k_B$  is the Boltzmann constant,  $T$  is the temperature and  $b$  is the bead size (segment size).  $N_s$  is a parameter which represents the strength of the slip-springs. As mentioned, the total number of slip-springs,  $Z$ , is not constant but fluctuates in time since slip-springs are dynamically constructed or destructed. To handle such a variable, it is convenient to use grand canonical type ensemble for slip-springs, which is originally introduced by Schieber [37] for the slip-link model. The grand potential of the system can be expressed as follows.

$$\mathcal{J}(\{\mathbf{R}_i\}, \{\mathbf{A}_j\}, \{S_j\}, Z) = \mathcal{F}(\{\mathbf{R}_i\}, \{\mathbf{A}_j\}, \{S_j\}, Z) - \nu Z \quad (2)$$

where  $\nu$  is the effective chemical potential for a slip-spring. As long as the detailed balance condition is satisfied, all the equilibrium statistical properties can be calculated from the grand potential (2). As we discuss later, we can design dynamics to satisfy the detailed balance condition, and thus all the equilibrium properties shown in the followings can be also applied to our dynamics model.

Before performing numerical simulations, we analytically show several equilibrium statistical properties of our single chain slip-spring model. In this section, we show equilibrium and linear-response properties. Here we may emphasize that the results in this section is based on the usual equilibrium statistical physics and the linear response theory in non-equilibrium statistical physics. As long as the detailed balance condition holds, all the results in this section also hold.

By using the grand potential (2), we can calculate the grand partition function of the system.

$$\begin{aligned} \Xi &\equiv \sum_{Z=0}^{\infty} \frac{1}{\Lambda^{3N} \Lambda_s^{3Z} Z!} \sum_{\{S_j\}} \int d\{\mathbf{R}_i\} d\{\mathbf{A}_j\} \left[ -\frac{\mathcal{J}(\{\mathbf{R}_i\}, \{\mathbf{A}_j\}, \{S_j\}, Z)}{k_B T} \right] \\ &= \frac{V}{\Lambda^3} \left( \frac{2\pi b^2}{3\Lambda^2} \right)^{3(N-1)/2} \exp \left[ N e^{\nu/k_B T} \left( \frac{2\pi N_s b^2}{3\Lambda_s^2} \right)^{3/2} \right] \end{aligned} \quad (3)$$

where  $V$  is the system volume.  $\Lambda$  and  $\Lambda_s$  are the thermal de Broglie wave lengths for a bead and a slip-spring, respectively. (They are required to make the grand partition function dimensionless. As we will show, thermodynamic properties are not affected by them.) The factorial  $Z!$  is the Gibbs factor due to the indistinguishability of slip-springs. The equilibrium distribution of a state is given as the following usual Boltzmann form.

$$P_{\text{eq}}(\{\mathbf{R}_i\}, \{\mathbf{A}_j\}, \{S_j\}, Z) = \frac{1}{\Xi} \frac{1}{\Lambda^{3N} \Lambda_s^{3Z} Z!} \exp \left[ -\frac{\mathcal{J}(\{\mathbf{R}_i\}, \{\mathbf{A}_j\}, \{S_j\}, Z)}{k_B T} \right] \quad (4)$$

Here the equilibrium distribution function is normalized to satisfy the following normalization condition.

$$\sum_{\{S_j\}, Z} \int d\{\mathbf{R}_i\}, d\{\mathbf{A}_j\} P_{\text{eq}}(\{\mathbf{R}_i\}, \{\mathbf{A}_j\}, \{S_j\}, Z) = 1 \quad (5)$$

The equilibrium average or distribution of a given set of variables can be calculated from eq (4). The equilibrium distribution of the chain conformation (the bead positions  $\{\mathbf{R}_i\}$ ),  $P_{\text{eq}}(\{\mathbf{R}_i\})$ , becomes

$$\begin{aligned} P_{\text{eq}}(\{\mathbf{R}_i\}) &= \sum_{\{S_j\}, Z} \int d\{\mathbf{A}_j\} P_{\text{eq}}(\{\mathbf{R}_i\}, \{\mathbf{A}_j\}, \{S_j\}, Z) \\ &= \frac{1}{V} \left( \frac{3}{2\pi b^2} \right)^{3(N-1)/2} \exp \left[ -\sum_{i=1}^{N-1} \frac{3}{2b^2} (\mathbf{R}_{i+1} - \mathbf{R}_i)^2 \right] \end{aligned} \quad (6)$$

Eq (6) is the same as the equilibrium conformation of an ideal chain. Thus we find that in equilibrium our model can be reduced to a single ideal chain. Therefore all the equilibrium statistical properties of a chain (such as the average end to end vector or the average radius of gyration) are just the same as ones of an ideal chain. This is consistent with the fact that the entanglement effect is just a dynamic effect and does not affect static properties.

Similarly, we can calculate equilibrium statistical properties of slip-springs. The equilibrium distribution of the number of slip-springs,  $P_{\text{eq}}(Z)$ , is given as follows.

$$\begin{aligned} P_{\text{eq}}(Z) &= \sum_{\{S_j\}} \int d\{\mathbf{R}_i\} d\{\mathbf{A}_j\} P_{\text{eq}}(\{\mathbf{R}_i\}, \{\mathbf{A}_j\}, \{S_j\}, Z) \\ &= \frac{1}{Z!} \exp \left[ \frac{\tilde{\nu}Z}{k_B T} - e^{\tilde{\nu}/k_B T} \right] \end{aligned} \quad (7)$$

where we defined the modified effective chemical potential  $\tilde{\nu}$  as

$$\tilde{\nu} \equiv \nu + k_B T \ln \left[ N \left( \frac{2\pi N_s b^2}{3\Lambda_s^2} \right)^{3/2} \right] \quad (8)$$

From eq (7) we find that the equilibrium distribution of  $Z$  is expressed as a Poisson distribution. This is consistent with the distribution function in the slip-link model by Schieber [37]. The average number of slip-springs  $\langle Z \rangle_{\text{eq}}$  ( $\langle \dots \rangle_{\text{eq}}$  means the equilibrium statistical average) can be related to the modified effective chemical potential  $\tilde{\nu}$ .

$$\langle Z \rangle_{\text{eq}} = \sum_{Z=0}^{\infty} Z P_{\text{eq}}(Z) = e^{\tilde{\nu}/k_B T} \quad (9)$$

We expect that the average number of slip-springs can be expressed by using the characteristic number of beads between slip-springs,  $N_0$ .

$$\langle Z \rangle_{\text{eq}} = \frac{N}{N_0} \quad (10)$$

Here we note that generally  $N_0$  in eq (10) does not coincide with the number of beads between entanglements calculated from the plateau modulus,  $N_e$ . (Typically  $N_0$  is smaller than  $N_e$  [10, 38].) From eqs (9) and (10), we have the following relation between  $N_0$  and  $\tilde{\nu}$ .

$$\tilde{\nu} = k_B T \ln \frac{N}{N_0} \quad (11)$$

Eq (7) can be then rewritten simply as

$$P_{\text{eq}}(Z) = \frac{1}{Z!} \left( \frac{N}{N_0} \right)^Z e^{-N/N_0} \quad (12)$$

By using eqs (6) and (12), we can rewrite eq (4) as follows.

$$P_{\text{eq}}(\{\mathbf{R}_i\}, \{\mathbf{A}_j\}, \{S_j\}, Z) = P_{\text{eq}}(\{\mathbf{R}_i\}) P_{\text{eq}}(Z) \prod_{j=1}^Z P_{\text{eq}}(S_j) P_{\text{eq}}(\mathbf{A}_j | \{\mathbf{R}_i\}, S_j) \quad (13)$$

$$P_{\text{eq}}(S_j) \equiv \frac{1}{N} \quad (14)$$

$$P_{\text{eq}}(\mathbf{A}_j | \{\mathbf{R}_i\}, S_j) \equiv \left( \frac{3}{2\pi N_s b^2} \right)^{3/2} \exp \left[ -\frac{3}{2N_s b^2} (\mathbf{R}_{S_j} - \mathbf{A}_j)^2 \right] \quad (15)$$

Here, the notation  $P_{\text{eq}}(X|Y)$  represents the conditional probability of  $X$  for given  $Y$ . Eq (14) is the equilibrium distribution of a bead index of a slip-spring. Eq (14) can be interpreted as

the equilibrium distribution of an ideal gas particle on a one dimensional lattice which has  $N$  lattice points. Eq (15) is the equilibrium distribution of an anchoring point under a given chain conformation and a bead index.

To study rheological properties, we need the microscopic expression for the stress tensor. From the stress-optical rule, the stress tensor of a single chain can be expressed by using the bead positions.

$$\boldsymbol{\sigma}(\{\mathbf{R}_i\}) = \sum_{i=1}^{N-1} \frac{3k_B T}{b^2} (\mathbf{R}_{i+1} - \mathbf{R}_i)(\mathbf{R}_{i+1} - \mathbf{R}_i) - Nk_B T \mathbf{1} \quad (16)$$

The second term in the right hand side of eq (16) does not have the non-diagonal elements and thus it can be dropped when we consider the shear stress or the normal stress difference. In equilibrium, the stress tensor of the system can be calculated to be

$$c_0 \langle \boldsymbol{\sigma}(\{\mathbf{R}_i\}) \rangle_{\text{eq}} = -c_0 k_B T \mathbf{1} \quad (17)$$

where  $c_0$  is the average density of polymer chains. ( $c_0$  can be related to the average bead density  $\rho_0$  as  $c_0 = \rho_0/N$ ). From eq (17) we find that in equilibrium, our single chain slip-spring model gives the stress tensor of an ideal gas system with the number density  $c_0$ . This is physically natural because the entanglement effect is purely kinetic, and the system is the same as a non-interacting Rouse chain system in equilibrium.

## 2.2 Dynamics

We cannot study dynamical properties only from the grand potential (2). In this subsection, we introduce a simple but physically valid dynamics model for a single chain slip-spring model. As we mentioned, the purpose of this work is to design a simulation model which is suitable for the calculations on a GPU. In this work, we will employ the CUDA programming model [26–28] which is developed and provided by NVIDIA corporation and widely used for GPGPU calculations.

Although the CUDA programming model provides us a fast and efficient GPGPU environment, there are several (rather strict) limitations. Before we design the dynamics model, here we briefly review some restrictions in CUDA which are directly related to the design of our dynamics model. First, parallel threads on a GPU are segmented into several blocks (each block contains typically from several tens to several hundreds of threads). The data communication between different blocks are much slower compared with the communication inside a block. Thus the data communication between blocks should be reduced to achieve high performance. Second, parallel threads are basically designed to perform the same task (with different data values) and the complicated conditional branches decrease the performance. Third, the amount of registers and shared memory is not large (the total registers and shared memory are 8192 (32kB) and 16kB per one block, respectively). Fourth, some arithmetic operations are not implemented, or not efficient compared with a CPU. (Although these restrictions depend on the GPU architecture, there are qualitatively similar restrictions for other GPGPU calculation models.) The dynamics model shown in this subsection is designed to achieve high performance calculations on a GPU under these limitations (see Section 3.2).

Although we introduce a specific dynamics model in this subsection, equilibrium properties (shown in the previous subsection) are not altered for other dynamics models as long as the detailed balance condition is satisfied.

We start from the dynamics of beads. In the absence of slip-springs ( $Z = 0$ ), we expect that the dynamics reduces to the Rouse dynamics. Then the dynamics of beads can be modelled as the simple Rouse type dynamics. We use an overdamped Langevin equation as the dynamic equation for a bead.

$$\frac{d\mathbf{R}_i(t)}{dt} = -\frac{1}{\zeta} \frac{\partial \mathcal{J}(\{\mathbf{R}_i\}, \{\mathbf{A}_j\}, \{S_j\}, Z)}{\partial \mathbf{R}_i} + \boldsymbol{\kappa}(t) \cdot \mathbf{R}_i + \boldsymbol{\xi}_i(t) \quad (18)$$

where  $\zeta$  is the friction coefficient for a bead,  $\boldsymbol{\kappa}(t)$  is the velocity gradient tensor, and  $\boldsymbol{\xi}_i(t)$  is the Gaussian white noise.  $\boldsymbol{\xi}_i(t)$  satisfies the following fluctuation-dissipation relation which guarantees

the detailed balance.

$$\langle \boldsymbol{\xi}_i(t) \rangle = 0 \quad (19)$$

$$\langle \boldsymbol{\xi}_i(t) \boldsymbol{\xi}_j(t') \rangle = \frac{2k_B T}{\zeta} \delta_{ij} \delta(t - t') \mathbf{1} \quad (20)$$

where  $\langle \dots \rangle$  means the statistical average and  $\mathbf{1}$  is the unit tensor.

Dynamics of slip-springs is not trivial. Because we are seeking a model which is suitable for simulations on a GPU, here we employ rather simple dynamics for slip-springs. We assume that the anchoring point of a slip-spring moves only by the external flow. Thus the dynamic equation for  $\mathbf{A}_j$  becomes the following simple advection equation.

$$\frac{d\mathbf{A}_j(t)}{dt} = \boldsymbol{\kappa}(t) \cdot \mathbf{A}_j \quad (21)$$

In the absence of the velocity gradient, the anchoring points do not change their positions unless they are reconstructed. For the dynamics of slip-spring bead indices, we employ stochastic jump processes [9, 39]. For simplicity, we assume that a slip-spring bead index can move only to its neighboring bead indices by a single jump. The jump probability from the bead index  $S_j$  to the bead index  $S'_j$  can be expressed as a transition matrix  $W(S'_j|S_j)$ .

$$W_S(S'_j|S_j) = \begin{cases} W_{S+}(S_j) & (S'_j = S_j + 1) \\ W_{S-}(S_j) & (S'_j = S_j - 1) \\ -W_{S+}(S_j) - W_{S-}(S_j) & (S'_j = S_j) \\ 0 & (\text{otherwise}) \end{cases} \quad (22)$$

where  $W_{S+}(S_j)$  and  $W_{S-}(S_j)$  are transition probabilities which increment or decrement the bead index, respectively. These transition probabilities should satisfy the detailed balance condition. There are many possible forms for the transition probabilities which satisfies the detailed balance condition. In this work we employ the following Glauber type dynamics [40]. (It is well known that the Glauber dynamics satisfies the detailed balance condition.)

$$W_{S+}(S_j) = \begin{cases} \frac{k_B T}{\zeta_s} \left[ 1 - \tanh \left[ \frac{3}{4N_s b^2} [(\mathbf{R}_{S_j+1} - \mathbf{A}_j)^2 - (\mathbf{R}_{S_j} - \mathbf{A}_j)^2] \right] \right] & (S_j < N) \\ 0 & (S_j = N) \end{cases} \quad (23)$$

$$W_{S-}(S_j) = \begin{cases} \frac{k_B T}{\zeta_s} \left[ 1 - \tanh \left[ \frac{3}{4N_s b^2} [(\mathbf{R}_{S_j-1} - \mathbf{A}_j)^2 - (\mathbf{R}_{S_j} - \mathbf{A}_j)^2] \right] \right] & (S_j > 1) \\ 0 & (S_j = 1) \end{cases} \quad (24)$$

Here  $\zeta_s$  is a parameter which represents the effective friction coefficient for a slip-spring. In contrast to the Likhtman's model, we allow slip-springs to pass through each other. However, as mentioned by Likhtman, this does not affect physical properties qualitatively. From the view point of numerical calculations, this enables numerical schemes to be simple and thus we can make the implementation on a GPU simple.

Finally we model the slip-spring reconstruction dynamics. Slip-springs on chain ends ( $S_j = 1, N$ ) can be removed from a chain and destructed. To compensate the destruction process, we have to introduce the slip-spring construction process on chain ends. These reconstruction events can be modelled as the jump processes, just like the dynamics for  $\{S_j\}$ . If we assume that just one slip-spring can be destructed or constructed at one reconstruction event, the jump probabilities become as follows.

$$W_Z(Z'|Z) = \begin{cases} W_{Z+}(Z) & (Z' = Z + 1) \\ W_{Z-}(Z) & (Z' = Z - 1) \\ -W_{Z+}(Z) - W_{Z-}(Z) & (Z' = Z) \\ 0 & (\text{otherwise}) \end{cases} \quad (25)$$

where  $W_{Z+}(Z)$  and  $W_{Z-}(Z)$  are the construction and destruction probabilities, respectively. From the detailed balance condition, they should satisfy the following relation.

$$W_{Z+}(Z)P_{\text{eq}}(\{\mathbf{R}_i\}, \{\mathbf{A}_j\}, \{S_j\}, Z) = W_{Z-}(Z)P_{\text{eq}}(\{\mathbf{R}_i\}, \{\mathbf{A}_j\}, \{S_j\}, Z+1) \quad (26)$$

Although the condition (26) limits the form of dynamics, there are still many possible candidates for the reconstruction probabilities. In this work, we employ the following rather simple jump probabilities for the slip-spring reconstruction process.

$$W_{Z+}(Z) = \frac{k_B T}{\zeta_s} (\delta_{S_{Z+1},1} + \delta_{S_{Z+1},N}) \frac{1}{N_0} \left( \frac{3}{2\pi N_s b^2} \right)^{3/2} \exp \left[ -\frac{3}{2N_s b^2} (\mathbf{R}_{S_{Z+1}} - \mathbf{A}_{Z+1})^2 \right] \quad (27)$$

$$W_{Z-}(Z) = \frac{k_B T}{\zeta_s} \sum_{j=1}^Z (\delta_{S_j,1} + \delta_{S_j,N}) \quad (28)$$

It is straightforward to show that eqs (27) and (28) together with eq (13) satisfy the condition (26). As we will show later, the transition probabilities (27) and (28) enable simple numerical implementations which are suitable to simulations on a GPU.

The single chain slip-spring model shown in this subsection can reproduce reptation type dynamics [1] qualitatively. We emphasize that each dynamics described in this subsection satisfies the detailed balance condition, and thus our single chain slip-spring model has well-defined thermodynamic equilibrium state.

Although we did not incorporate the effects such as the constraint release (CR) or the convective constraint release (CCR) into our model, it is not difficult to take these effects and improve the model. Interestingly, while the CR process is not explicitly considered, the relaxation process which is qualitatively similar to the CR exists in our model. (As shown in Appendix A, the dynamics of bead indices exhibit CR type relaxation mechanism.) Our model can reproduce rheological properties reasonably, as we will show later.

### 2.3 Linear Response Theory

To obtain linear response functions such as the shear relaxation modulus around equilibrium, the linear response theory [41] is sometimes quite useful. The linear response theory states that if the dynamics satisfies the detailed balance condition, the response of the system to a small perturbation is simply expressed by correlation functions (the fluctuation-dissipation relation). Because our model is designed to satisfy the detailed balance condition, we can utilize the fluctuation-dissipation relation to calculate the response in our model. (Some slip-link models do not satisfy the detailed balance condition. For such models, the validity of the linear response theory is not guaranteed and it may not be useful.) In this subsection, we show the explicit expression for the relaxation modulus by using the standard linear response theory.

The dynamics of our single chain slip-spring model is described by the Langevin equation and jump processes. In the absence of the velocity gradient tensor the system can relax to the equilibrium state, because the detailed balance condition is satisfied. Now we consider the velocity gradient tensor,  $\boldsymbol{\kappa}(t)$ , as a time-dependent small perturbation and calculate the response of the time-dependent stress tensor  $\boldsymbol{\sigma}(t)$  to  $\boldsymbol{\kappa}(t)$ .

The probability distribution function is useful to calculate the linear response. We define the time-dependent probability distribution function in the phase space as

$$P(\{\mathbf{r}_i\}, \{\mathbf{a}_i\}, \{s_i\}, z; t) \equiv \left\langle \delta_{z,Z(t)} \left[ \prod_{i=1}^N \delta(\mathbf{r}_i - \mathbf{R}_i(t)) \right] \left[ \prod_{j=1}^z \delta_{s_j, S_j(t)} \delta(\mathbf{a}_j - \mathbf{A}_j(t)) \right] \right\rangle \quad (29)$$

The time evolution of the probability distribution function can be given as the following master equation.

$$\frac{\partial}{\partial t} P(\{\mathbf{r}_i\}, \{\mathbf{a}_j\}, \{s_j\}, z; t) = [\mathcal{L}_{\mathbf{R}}(t) + \mathcal{L}_{\mathbf{A}}(t) + \mathcal{L}_S + \mathcal{L}_Z] P(\{\mathbf{r}_i\}, \{\mathbf{a}_j\}, \{s_j\}, z; t) \quad (30)$$

where  $\mathcal{L}_{\mathbf{R}}(t)$  and  $\mathcal{L}_{\mathbf{A}}(t)$  are the Fokker-Planck type operators, and  $\mathcal{L}_S$  and  $\mathcal{L}_Z$  are the time evolution operators which come from jump processes for  $\{S_j\}$  and  $Z$ . Notice that  $\mathcal{L}_{\mathbf{R}}(t)$  and  $\mathcal{L}_{\mathbf{A}}(t)$  depend on time  $t$  whereas  $\mathcal{L}_S$  and  $\mathcal{L}_Z$  do not. This is because the dynamics of  $\{S_j\}$  and  $Z$  is not directly affected by the external flow. The explicit forms for  $\mathcal{L}_{\mathbf{R}}(t)$  and  $\mathcal{L}_{\mathbf{A}}(t)$  are as follows.

$$\mathcal{L}_{\mathbf{R}}(t)P = \sum_{i=1}^N \frac{1}{\zeta} \frac{\partial}{\partial \mathbf{r}_i} \cdot \left[ \frac{\partial \mathcal{J}(\{\mathbf{r}_i\}, \{\mathbf{a}_j\}, \{s_j\}, z)}{\partial \mathbf{r}_i} P - \zeta \boldsymbol{\kappa}(t) \cdot \mathbf{r}_i P + k_B T \frac{\partial P}{\partial \mathbf{r}_i} \right] \quad (31)$$

$$\mathcal{L}_{\mathbf{A}}(t)P = - \sum_{j=1}^Z \frac{\partial}{\partial \mathbf{a}_j} \cdot [\boldsymbol{\kappa}(t) \cdot \mathbf{a}_j P] \quad (32)$$

We do not show the explicit forms for  $\mathcal{L}_S$  and  $\mathcal{L}_Z$  here, because their explicit forms are not required in the following calculations.

To calculate the linear response, we need to decompose the time evolution operator into the equilibrium and perturbation parts. Thus we define the following two time evolution operators.

$$\mathcal{L}_0 P \equiv \sum_{i=1}^N \frac{1}{\zeta} \frac{\partial}{\partial \mathbf{r}_i} \cdot \left[ \frac{\partial \mathcal{J}}{\partial \mathbf{r}_i} P + k_B T \frac{\partial P}{\partial \mathbf{r}_i} \right] + \mathcal{L}_S P + \mathcal{L}_Z P \quad (33)$$

$$\mathcal{L}_1(t)P \equiv - \sum_{i=1}^N \frac{\partial}{\partial \mathbf{r}_i} \cdot [\boldsymbol{\kappa}(t) \cdot \mathbf{r}_i P] - \sum_{j=1}^Z \frac{\partial}{\partial \mathbf{a}_j} \cdot [\boldsymbol{\kappa}(t) \cdot \mathbf{a}_j P] \quad (34)$$

By using these operators, the time evolution equation of the probability distribution function can be simply described as follows.

$$\frac{\partial P}{\partial t} = [\mathcal{L}_0 + \mathcal{L}_1(t)]P \quad (35)$$

In the absence of the velocity gradient, the perturbation part of the time evolution operator disappears ( $\mathcal{L}_1(t) = 0$ ) and the system relaxes to the equilibrium state. The equilibrium distribution function  $P_{\text{eq}}$  is given as the Boltzmann form since the detailed balance condition is satisfied.

$$P_{\text{eq}}(\{\mathbf{r}_i\}, \{\mathbf{a}_i\}, \{s_i\}, z) \equiv \frac{1}{\Xi} \frac{1}{\Lambda^{3N} \Lambda_s^{3z} z!} \exp \left[ - \frac{\mathcal{J}(\{\mathbf{r}_i\}, \{\mathbf{a}_i\}, \{s_i\}, z)}{k_B T} \right] \quad (36)$$

Using the equilibrium distribution function we write the equilibrium average for an operator  $\hat{B}$  as

$$\langle \hat{B} \rangle_{\text{eq}} \equiv \sum_{z, \{s_j\}} \int d\{\mathbf{r}_i\} d\{\mathbf{a}_j\} \hat{B} P_{\text{eq}}(\{\mathbf{r}_i\}, \{\mathbf{a}_i\}, \{s_i\}, z) \quad (37)$$

Now we can follow the standard procedure to calculate the linear response [41, 42]. The time-dependent stress tensor of a single chain is calculated by the following stress tensor operator.

$$\hat{\boldsymbol{\sigma}} \equiv \sum_{i=1}^{N-1} \frac{3k_B T}{b^2} (\mathbf{r}_{i+1} - \mathbf{r}_i)(\mathbf{r}_{i+1} - \mathbf{r}_i) - Nk_B T \mathbf{1} \quad (38)$$

Following the standard linear response theory, we have the following expression for the time-dependent stress tensor. (See Appendix B for detail.)

$$\begin{aligned} \boldsymbol{\sigma}(t) &= \sum_{z, \{s_j\}} \int d\{\mathbf{r}_i\} d\{\mathbf{a}_j\} \hat{\boldsymbol{\sigma}} P(\{\mathbf{r}_i\}, \{\mathbf{a}_j\}, \{s_j\}, z; t) \\ &= \boldsymbol{\sigma}_{\text{eq}} + \int_{-\infty}^t dt' \sum_{z, \{s_i\}} \int d\{\mathbf{r}_i\} d\{\mathbf{a}_i\} \hat{\boldsymbol{\sigma}} e^{(t-t')\mathcal{L}_0} \mathcal{L}_1(t') P_{\text{eq}} \end{aligned} \quad (39)$$



where  $\boldsymbol{\sigma}_{\text{eq}} \equiv \langle \hat{\boldsymbol{\sigma}} \rangle_{\text{eq}} = -k_B T \mathbf{1}$  is the equilibrium value of the stress tensor. After straightforward calculations, finally we have the following expression for the time-dependent stress tensor.

$$\boldsymbol{\sigma}(t) = \boldsymbol{\sigma}_{\text{eq}} + \frac{1}{k_B T} \int_{-\infty}^t dt' \left[ \langle \hat{\boldsymbol{\sigma}}(t-t') \hat{\boldsymbol{\sigma}} \rangle_{\text{eq}} + \langle \hat{\boldsymbol{\sigma}}(t-t') \hat{\boldsymbol{\sigma}}^{(v)} \rangle_{\text{eq}} \right] : \boldsymbol{\kappa}(t') \quad (40)$$

where  $\hat{\boldsymbol{\sigma}}(t)$  is the stress tensor operator evolved by time  $t$  (the time-shifted stress tensor operator) and  $\hat{\boldsymbol{\sigma}}^{(v)}$  is the virtual stress tensor operator by slip-springs and  $:$  means the dyadic product.  $\hat{\boldsymbol{\sigma}}^{(v)}$  is defined as

$$\hat{\boldsymbol{\sigma}}^{(v)} \equiv \sum_{j=1}^{z-1} \frac{3k_B T}{N_s b^2} (\mathbf{r}_{s_j} - \mathbf{a}_j)(\mathbf{r}_{s_j} - \mathbf{a}_j) - z k_B T \mathbf{1} \quad (41)$$

Eq (41) is similar to eq (38) but it represents the contribution of slip-springs. The relaxation modulus tensor  $\mathbf{G}(t)$  (which is a fourth order tensor) corresponds to the response function of the stress to the velocity gradient. In this work we use the following definition for the relaxation modulus tensor.

$$c_0[\boldsymbol{\sigma}(t) - \boldsymbol{\sigma}_{\text{eq}}] = \int_{-\infty}^t dt' \mathbf{G}(t-t') : \boldsymbol{\kappa}(t') \quad (42)$$

From eqs (40) and (42), we find that the relaxation modulus tensor is simply given as

$$\mathbf{G}(t) = \frac{c_0}{k_B T} \langle \hat{\boldsymbol{\sigma}}(t) \hat{\boldsymbol{\sigma}} \rangle_{\text{eq}} + \frac{c_0}{k_B T} \langle \hat{\boldsymbol{\sigma}}(t) \hat{\boldsymbol{\sigma}}^{(v)} \rangle_{\text{eq}} \quad (43)$$

It should be noted here that there are two contributions for the relaxation modulus tensor. One is the usual stress-stress autocorrelation function, and another is the stress-virtual stress correlation function which does not appear in usual many body systems.

Here we note that eq (43) coincide with the formula previously proposed by Ramirez, Sukumaran and Likhtman [43]. Intuitively, this form can be understood as follows. The stress tensor operator  $\hat{\boldsymbol{\sigma}}$  is not conjugate to the perturbation  $\boldsymbol{\kappa}(t)$ , but the sum of the stress and the virtual stress operators,  $\hat{\boldsymbol{\sigma}} + \hat{\boldsymbol{\sigma}}^{(v)}$ , is conjugate to the perturbation. Then, following the standard formula of the linear response theory, the response function is given as the time correlation function of  $\hat{\boldsymbol{\sigma}}$  and  $\hat{\boldsymbol{\sigma}} + \hat{\boldsymbol{\sigma}}^{(v)}$ , which gives eq (40). If we employ  $\hat{\boldsymbol{\sigma}} + \hat{\boldsymbol{\sigma}}^{(v)}$  as the stress tensor of a chain, the relaxation modulus tensor is simply given as the autocorrelation function of  $\hat{\boldsymbol{\sigma}} + \hat{\boldsymbol{\sigma}}^{(v)}$ . However, such a definition violates the stress-optical rule, and it is physically unnatural. (We will examine the contribution of the virtual stress is quantitatively, later.) Therefore, in this work we use  $\hat{\boldsymbol{\sigma}}$  as the stress tensor operator.

## 3 Numerical Scheme and Implementation

### 3.1 Discretization Scheme

To solve dynamics of our single chain slip-spring model numerically, we need to discretize dynamic equations and jump processes. In this subsection, we briefly show the discretization scheme. Since our purpose in this work is to develop a model which is suitable for calculations on a GPU, here we aim to make rather simple and stable schemes.

Before considering discretization schemes, we make all the parameters dimensionless. We set  $b = 1$ ,  $k_B T = 1$ , and  $\zeta = 1$ . (This is equivalent to make all the dimensional parameters dimensionless by characteristic scales  $b$ ,  $k_B T$ , and  $\zeta$ .) The characteristic time scale of simulations also becomes unity ( $\tau_0 \equiv \zeta b^2 / k_B T = 1$ ).

To make schemes simpler, we split dynamics from  $t$  to  $t + \Delta t$  (with  $\Delta t$  being the time step size) into several substeps. In this work, we use the following three substeps to evolve the system from  $t$  to  $t + \Delta t$ . Each substep is designed to satisfy the detailed balance condition for small  $\Delta t$  ( $\Delta t \ll 1$ ).

1. Integrate dynamics equations for  $\{\mathbf{R}_i\}, \{\mathbf{A}_j\}$  (eqs (18) and (21)). These are stochastic differential equation and ordinary differential equation and thus we can employ several standard schemes. To minimize the computational cost, here we employ the explicit Euler method which is not accurate but the simplest.

$$\mathbf{R}_i(t + \Delta t) = -\Delta t \frac{\partial \mathcal{J}(\{\mathbf{R}_i\}, \{\mathbf{A}_j\}, \{S_i\}, Z)}{\partial \mathbf{R}_i} + \Delta t \boldsymbol{\kappa}(t) \cdot \mathbf{R}_i + \sqrt{2\Delta t} \mathbf{w}_i \quad (44)$$

$$\mathbf{A}_j(t + \Delta t) = \Delta t \boldsymbol{\kappa}(t) \cdot \mathbf{A}_j \quad (45)$$

where  $\mathbf{w}_i$  is a standard distribution random number vector which satisfies the following relation.

$$\langle \mathbf{w}_i \rangle = 0 \quad (46)$$

$$\langle \mathbf{w}_i \mathbf{w}_j \rangle = \delta_{ij} \mathbf{1} \quad (47)$$

$\mathbf{w}_i$  can be generated easily by some random number generators such as the combination of the linear coagulation method and the Box-Muller transform.

2. Move slip-spring bead indices  $\{S_j\}$  by transition probabilities (22)-(24). We use the following accumulated probabilities for finite time step  $\Delta t$  and uniform distribution random variables.

$$P(S_j \rightarrow S_j + 1) = \begin{cases} \min \left\{ \frac{\Delta t}{\zeta_s} \left[ 1 - \tanh \left[ \frac{3}{4N_s} [(\mathbf{R}_{S_{j+1}} - \mathbf{A}_j)^2 - (\mathbf{R}_{S_j} - \mathbf{A}_j)^2] \right] \right], \frac{1}{2} \right\} & (S_j < N) \\ 0 & (S_j = N) \end{cases} \quad (48)$$

$$P(S_j \rightarrow S_j - 1) = \begin{cases} \min \left\{ \frac{\Delta t}{\zeta_s} \left[ 1 - \tanh \left[ \frac{3}{4N_s} [(\mathbf{R}_{S_{j-1}} - \mathbf{A}_j)^2 - (\mathbf{R}_{S_j} - \mathbf{A}_j)^2] \right] \right], \frac{1}{2} \right\} & (S_j > 1) \\ 0 & (S_j = 1) \end{cases} \quad (49)$$

The minima are taken so that each transition probability does not exceed 1/2. Although the discretization scheme shown here is not accurate, it does not fail even for large  $\Delta t$  due to this trick.

3. Reconstruct slip-springs on chain ends by the transition probability eq (25), (27), and (28). First, new slip-springs are constructed at chain ends by the following accumulated probability. The construction is attempted  $K$  times repeatedly (with  $K$  being an integer parameter which can depend on  $Z$ ). This parameter  $K$  is introduced to allow the construction attempt evaluated in parallel. This is because parallel attempts are much efficient than single attempt on a GPU. (See Section 3.2.)

$$P_{\text{construct}}(S_{Z+1} = 1) = \min \left\{ \frac{\Delta t}{\zeta_s} \frac{1}{N_0} \frac{1}{K}, \frac{1}{2} \right\} \quad (50)$$

$$P_{\text{construct}}(S_{Z+1} = N) = \min \left\{ \frac{\Delta t}{\zeta_s} \frac{1}{N_0} \frac{1}{K}, \frac{1}{2} \right\} \quad (51)$$

The minima are taken to prevent each transition probability from exceeding 1/2. The anchored point position of a new slip-spring,  $\mathbf{A}_{Z+1}$ , is sampled from the equilibrium distribution. Since the equilibrium distribution of an anchoring point is Gaussian (eq (15)), it can be easily generated.

$$P_{\text{construct}}(\mathbf{A}_{Z+1}) = \left( \frac{3}{2\pi N_s} \right)^{3/2} \exp \left[ -\frac{3}{2N_s} (\mathbf{R}_{S_{Z+1}} - \mathbf{A}_{Z+1})^2 \right] \quad (52)$$

Second, each slip-spring is destructed by the following accumulated probability.

$$P_{\text{destruct}}(S_j) = \min \left\{ \frac{\Delta t}{\zeta_s} (\delta_{S_j,1} + \delta_{S_j,N}), 1 \right\} \quad (53)$$

As before, the minimum is taken to avoid each transition probability to exceed 1. We reset indices of slip-springs after the constructions or destructions. This ensures that the index for slip-springs on a chain always runs from 1 to  $Z$  ( $j = 1, 2, \dots, Z$ ).

The discretization schemes shown here are not accurate compared with more advanced schemes. (For example, it is possible to improve the accuracy by employing more advanced and accurate discretization schemes such as the stochastic Runge-Kutta method [44].) In this work, we prefer inaccurate but simple schemes for an implementation on a GPU. Since discretization schemes are designed to be as simple as possible, it is not difficult to implement them for GPGPU calculations (in which we have several limitations due to the GPU architecture). Although the accuracy is not high, we can perform stable simulations with these schemes even for not small  $\Delta t$ . (That is, the simulations do not fail easily even for rather large  $\Delta t$ .)

Before starting simulations we have to prepare well equilibrated samples. Since we know the equilibrium probability distribution, we can directly generate the equilibrium conformation of chains and slip-springs easily. All the simulations performed in this work start from the equilibrium state generated based on eq (13). The sampling procedure is as follows.

1. Generate polymer conformation  $\{\mathbf{R}_i\}$  by sampling from the Gaussian distribution (eq (6)).
2. Sample  $Z$  from the Poisson distribution (eq (12)).
3. Generate  $Z$  slip-springs. Each segment index,  $S_j$ , is sampled from the uniform distribution (eq (14)) and each anchoring point,  $\mathbf{A}_j$ , is sampled from the Gaussian distribution (eq (15)).

To obtain statistical quantities from Langevin type simulations, we need to perform many simulations with the same parameter set and different random number series. For this purpose, we simulate  $M$  different polymer chains and calculate the statistical average of an arbitrary physical quantity  $B$  approximately as

$$\langle B \rangle \approx \frac{1}{M} \sum_{k=1}^M B(\{\mathbf{R}_{k,i}\}, \{\mathbf{A}_{k,j}\}, \{S_{k,j}\}, Z_k) \quad (54)$$

where the subscript  $k$  means that the variable is of the  $k$ -th sample chain (for example,  $\mathbf{R}_{k,i}$  is the  $i$ -th bead position of the  $k$ -th chain).

### 3.2 Implementation on GPU

As we mentioned, we use the CUDA programming model to implement the discretized single chain slip-spring model on a GPU. In the CUDA programming model, there are two memory spaces on a graphics card; the global memory and the shared memory. The shared memory is small (currently its size is just 16kB) but the access speed is fast (comparable to the access speed of the registers). The global memory is large but the access speed is rather slow. Thus it is required to reduce the access to the global memory to speed up the program. Fortunately, our single chain slip-spring model requires very small memories and thus most of the data can be stored in the registers or the shared memory. To make the CUDA program efficient, it is also required to achieve high parallelism because a GPU has many threads (typically about several hundreds or several thousands) which are executed simultaneously. We can implement highly parallelized program by allocating one bead and one slip-spring to one CUDA thread. Although this limits the maximum number of slip-springs ( $Z \leq N$ ), in most cases it cause no problems (the probability that  $Z > N$  is practically negligible if  $N_0$  is not small). Here we note that, it is difficult to implement in such a way if we employ the slip-link type single chain model [6–9, 11], because nodes are dynamically reconstructed and thus

the number of total nodes is not constant. This is one of the main reason why the slip-spring model is employed in this work.

For the slip-spring reconstruction scheme on a GPU, we set the number of attempts to construct slip-springs as  $K = N - Z$ . This means that each thread which do not have a slip-spring attempts to construct a new one (and each attempt can be evaluated in parallel). For a CPU, we set  $K = 1$ , which means that the slip-spring construction is attempted only once at each step. Clearly this is suitable for a CPU, because we cannot evaluate many attempts in parallel. (Strictly speaking, this implementation will violate the detailed balance condition. But the violation is practically negligible.)

Currently it is generally not efficient to use double precision floating-point numbers (“double” type variables in CUDA), and thus single precision floating-point numbers (the “float” type variables) should be used to accelerate simulations efficiently. Fortunately this limitation is not serious for our single chain slip-spring model. Because our model is based on the stochastic differential equations and jump processes, the accuracy is mainly determined by number of samples and the error is typically much larger than the error of single precision floating-point number operations (the machine epsilon is about  $\epsilon_{\text{float}} \approx 10^{-7}$  whereas the statistical error is roughly proportional to the inverse square root of sampling numbers). Several elementary mathematical functions can be calculated very efficiently on a GPU. In our implementation, functions such as  $\sin x$ ,  $\cos x$ ,  $\exp x$ ,  $\ln x$ , or  $\sqrt{x}$  are used. Although the fast calculations for these mathematical functions involve some errors, such errors are not serious in our simulations (the errors are typically comparable to one of single precision floating-point number operations).

In parallelized programs, it is often needed to perform reduction operations. In our model, we have to calculate the total number of slip-springs on a chain or forces acting on beads caused by slip-springs. The reduction operations are one of the most time-consuming parts in our simulations. Although CUDA currently does not provide special functions for these reduction operations, we can use some techniques to improve the speed of the reduction operations [45].

Another time-consuming part is the calculation of the slip-spring force acting on a chain. To calculate the slip-spring force efficiently, we utilize the fixed-point real number technique [46] and the atomic operations [28] in CUDA. The fixed-point real number technique uses the integer type variable  $x$  as the real number  $y = x \times \epsilon_{\text{fixed}}$  with  $\epsilon_{\text{fixed}}$  being the resolution. The resolution  $\epsilon_{\text{fixed}}$  should be determined so that the truncation error is sufficiently small and the overflow does not occur. (Because the single precision float number has the machine epsilon  $\epsilon_{\text{float}} \approx 10^{-7}$ ,  $\epsilon_{\text{fixed}}$  is not necessarily to be very small.) In this work we set  $\epsilon_{\text{fixed}} = 1/4096 \approx 2.4 \times 10^{-4}$ , which has a sufficient resolution yet the overflow does not occur even under fast shear rates. The results shown below are not sensitive to the value of  $\epsilon_{\text{fixed}}$ , as long as  $\epsilon_{\text{fixed}}$  is not too small nor too large.

## 4 Results

### 4.1 Rheological Properties

Before measuring the acceleration effect by a GPU, we calculate several rheological properties of our slip-spring model. To obtain reliable simulation results, in this subsection, all the simulations are performed on a CPU. (The discretization schemes on a CPU are almost the same as the schemes on a GPU.) We set the simulation parameters as follows; the entanglement bead number  $N_0 = 4$ , slip-spring strength  $N_s = 0.5$ , the slip-spring friction coefficient  $\zeta_s = 0.1$ , and the time step size  $\Delta t = 0.01$ .

We first calculate the linear viscoelasticity by using the linear response formula (43). The storage and loss moduli,  $G'(\omega)$  and  $G''(\omega)$ , are then calculated by utilizing the following relations.

$$G'(\omega) = \omega \int_0^{\infty} dt G_{xyxy}(t) \sin(\omega t) \quad (55)$$

$$G''(\omega) = \omega \int_0^{\infty} dt G_{xyxy}(t) \cos(\omega t) \quad (56)$$

The integration in eqs (55) and (56) are numerically calculated by using the trapezoidal rule. Figure 1 shows the linear viscoelasticity data calculated from equilibrium single chain slip-springs simulations (for  $N = 10, 20, 40,$  and  $80$ ). Notice that  $G'(\omega)$  and  $G''(\omega)$  are normalized by  $\rho_0 k_B T$  to be dimensionless forms ( $\rho_0$  is the average bead density). As shown in Figure 1, our model reproduces linear viscoelasticity of entangled polymers qualitatively well, especially considering the simplicity of the model. The plateau modulus is about  $G_N^{(0)} \approx 0.1\rho_0 k_B T$ , which is almost the same as the plateau modulus obtained by the original slip-spring model simulation [10]. This means that, the characteristic number of beads between slip-springs  $N_0$  in this model is not identical to the entanglement bead number calculated from the plateau modulus based on the rubber elasticity theory. Following the standard definition, we define  $N_e$  via the following equation.

$$N_e \equiv \frac{\rho_0 k_B T}{G_N^{(0)}} \quad (57)$$

From  $G_N^{(0)} \approx 0.1\rho_0 k_B T$ , we have  $N_e \approx 10$ . This value is much larger than  $N_0$  ( $N_e \approx 2.5N_0$ ). Therefore the plateau modulus or  $N_e$  are not determined only by  $N_0$ , but they depends on various parameters in a rather complex way. Practically, it is reasonable to use both  $N_0$  and  $G_0$  (or  $G_N^{(0)}$ ) as two independent fitting parameters [10, 47].

Figure 2 shows the longest relaxation time calculated from the linear viscoelasticity data. The longest relaxation time is calculated via the following equation

$$\frac{1}{\tau_d} = - \lim_{t \rightarrow \infty} \frac{\ln G_{xyxy}(t)}{t} \quad (58)$$

For small  $N$ , we find that the longest relaxation time is proportional to  $(N - 1)^2$ , which agrees with the scaling of the Rouse relaxation time. (Here  $N - 1$  is used instead of  $N$ , since  $N - 1$  corresponds to the number of bonds in a chain [48].) This indicates that for small  $N$  (from Figure 2,  $N \lesssim 10$ ) a chain with slip-springs behave essentially as an unentangled chain. For large  $N$ , the relaxation time depends on  $N - 1$  as  $\tau_d \propto (N - 1)^{3.48}$ , which is similar to experimental results,  $\tau_d \propto (N - 1)^{3.4}$  (larger than the prediction of the pure reptation theory [1],  $\tau_d \propto (N - 1)^3$ ). Thus we find that the longest relaxation time and the zero shear is also reasonably reproduced by our simulation model.

Figure 3 shows the zero shear viscosity  $\eta_0$ . The zero shear viscosity is calculated from  $G(t)$  as

$$\eta_0 = \int_0^\infty dt G(t) \quad (59)$$

We find that the viscosity is proportional to  $N - 1$  or  $(N - 1)^{3.40}$  for small or large  $N$ , respectively. The cross over bead number is roughly estimated to be  $N_c \approx 14.2 \approx 1.4N_e$ . This value is slightly smaller than the experimental value  $N_c/N_0 = 1.6 \sim 3.5$  [49], but the discrepancy is not so large. Although we do not show simulation results for other parameter sets (for example, for different  $N_0$ ,  $N_s$ , or  $\zeta_s$ ), as shown in Ref 10, the effects of these parameters are not large and we have qualitatively similar results. Thus in this work we limit ourselves only to the standard parameter set used in Ref 10.

Next we calculate the viscosity growth  $\eta(t, \dot{\gamma})$  and the steady state viscosity  $\eta(\dot{\gamma})$ . At  $t = 0$ , the system is in equilibrium. For  $t > 0$  we apply the constant shear flow as

$$\kappa_{\alpha\beta} = \begin{cases} \dot{\gamma} & (\alpha = x, \beta = y) \\ 0 & (\text{otherwise}) \end{cases} \quad (60)$$

and calculate  $\eta(t, \dot{\gamma})$  and  $\eta(\dot{\gamma})$  as follows.

$$\eta(t, \dot{\gamma}) = \frac{\langle \sigma_{xy}(t) \rangle}{\dot{\gamma}} \quad (61)$$

$$\eta(\dot{\gamma}) = \lim_{t \rightarrow \infty} \eta(t, \dot{\gamma}) \quad (62)$$

We also calculate the dynamic viscosity, which is defined as follows, to check whether the Cox-Merz rule [50] holds or not.

$$\eta(\dot{\gamma}) \approx \eta^*(\omega)|_{\omega=\dot{\gamma}} \quad (63)$$

$$\eta^*(\omega) \equiv \sqrt{G'^2(\omega) + G''^2(\omega)} \quad (64)$$

Figure 4 shows the viscosity growth curves for  $N = 40$  with various shear rates ( $\dot{\gamma}\tau_0 = 0.0025, 0.005, 0.01, 0.025, 0.05, \text{ and } 0.1$ ). The number of sample chains is  $M = 1024$  for all shear rates. As shown in Figure 4, that viscosity growth curves can be qualitatively well reproduced by the single chain slip-spring model. The stress overshoot behavior and the shear thinning behavior are reasonably reproduced.

Figure 5 shows the dynamic and steady state viscosities calculated for  $N = 10, 20, 40, \text{ and } 80$ . For relatively small  $\dot{\gamma}$  and  $\omega$ , we observe that the Cox-Merz rule (63) holds reasonably. However, we find that in high shear rate regions, the steady state viscosities deviate from the complex viscosity and the Cox-Merz rule does not hold. In such regions, the viscosities are nearly independent of shear rate, thus they are the second Newtonian viscosities. These second Newtonian viscosities can be understood as follows. In high shear rate regions, slip-springs as well as chains are strongly stretched and slip-springs are easily destructed. Thus there are only a few slip-springs on a chain. For example, for  $N = 80$  ( $\langle Z \rangle_{\text{eq}} = 20$ ), the steady state average number of slip-springs are  $\langle Z \rangle = 8.7, 4.2, \text{ and } 1.6$  for  $\dot{\gamma} = 0.01, 0.1, \text{ and } 1$ , respectively. Then, a chain behaves essentially like an ideal, Rouse chain. The viscosity of a Rouse chain is independent of shear rate since the Rouse model is linear. Following this picture, we expect that the second Newtonian viscosity depends on  $N$  as

$$\frac{\eta(\dot{\gamma})}{\rho_0 k_B T \tau_0} \propto N \quad (65)$$

In Figure 5, we can observe that eq (65) approximately holds at the high shear rate region in Figure 5. Therefore we conclude that the second Newtonian like behavior in high shear rate region is an artifact of our model, rather than a physical property of an entangled chain. This means that our model should not be applied to very high shear rate regions where the Cox-Merz rule is violated. Results for the steady state viscosity may be utilized to validate simulation results under more complex situations, such as flows around obstacles.

In the shear thinning region in Figure 5, the steady state viscosity obeys the power law  $\eta(\dot{\gamma}) \propto \dot{\gamma}^{-\alpha}$ . The exponent  $\alpha$  is smaller than 1 and thus the steady state shear stress  $\sigma_{xy}(\dot{\gamma}) \propto \dot{\gamma}^{1-\alpha}$  is a monotonically increasing function of the shear rate  $\dot{\gamma}$ . In the simple Doi-Edwards type tube model [1],  $\sigma_{xy}(\dot{\gamma})$  is not a monotonically increasing function of  $\dot{\gamma}$ , and such a non-monotonic relation can cause mechanical instability (shear-banding instability) [51]. It is known that the CCR mechanism can successfully remove this instability [52, 53]. As we mentioned, the CR or CCR mechanisms are not explicitly taken into our model. Even in absence of the CCR mechanism, our model is free from the mechanical instability (at least in the investigated parameter range).

Finally, we shortly investigate the contribution of the virtual stress tensor  $\hat{\sigma}^{(v)}$ . In Section 2.3 we assumed that the stress tensor of the system is given by  $\hat{\sigma}$  defined by eq (38). One may prefer to employ  $\hat{\sigma} + \hat{\sigma}^{(v)}$  as the stress tensor of the system, which is conjugate to the velocity gradient tensor. Here we consider the shear relaxation modulus as an example. The relative contribution of the virtual stress to the shear relaxation modulus can be defined as

$$\Delta \tilde{G}^{(v)}(t) \equiv \frac{\langle \hat{\sigma}_{xy}^{(v)}(t) \hat{\sigma}_{xy} \rangle_{\text{eq}} + \langle \hat{\sigma}_{xy}^{(v)}(t) \hat{\sigma}_{xy}^{(v)} \rangle_{\text{eq}}}{\langle \hat{\sigma}_{xy}(t) \hat{\sigma}_{xy} \rangle_{\text{eq}} + \langle \hat{\sigma}_{xy}(t) \hat{\sigma}_{xy}^{(v)} \rangle_{\text{eq}}} \quad (66)$$

If  $\Delta \tilde{G}^{(v)}(t)$  is negligibly small, or if it is independent of  $t$ , the stress-optical rule approximately holds even if we employ  $\hat{\sigma} + \hat{\sigma}^{(v)}$  as the stress tensor of the system. Figure 6 shows the relative contribution of the virtual stress for  $N = 40$ . As shown in Figure 6,  $\Delta \tilde{G}^{(v)}(t)$  is roughly about 25% and this value is not negligibly small. However, it does not strongly depend on time  $t$ . This means that if we employ  $\hat{\sigma} + \hat{\sigma}^{(v)}$  as the stress tensor of the system, the stress-optical rule is approximately valid and rheological properties would be qualitatively not changed (quantitatively they would be

changed by about 25%). The results shown in this subsection are therefore qualitatively not sensitive to the definition of the stress tensor.

Judging from obtained rheological data, we can conclude that our model reasonably reproduces rheological properties and can be used to study rheological properties or flow behaviors of entangled polymers. Although further improvement of the model will be possible, it is beyond the scope of the current work and left for a future work.

## 4.2 Comparison of Rheological Properties with Original Slip-Spring Model

In this subsection, we briefly compare rheological data calculated by our single chain slip-spring model and the Likhtman’s original slip-spring model. We compare several rheology data shown in Ref 10 with the results of our simulations.

To avoid numerical errors due to the fitting or the numerical integration, we compare the shear relaxation modulus instead of storage and loss moduli. Figure 7(a) shows the shear relaxation moduli calculated by our model and the original slip-spring model, for  $N = 8, 16, 32, 64$  and 128. Other parameters ( $N_0, N_s$  and  $\zeta_s$ ) are the same. The data of the original model is taken from Fig. 4(a) of Ref 10. We can observe that the forms of  $G(t)$  calculated by our model and the original model are quite similar for long time region ( $t \gtrsim 10\tau_0$ ), while the longest relaxation times are quantitatively different. Our model gives longer relaxation time for all cases. We consider this is mainly due to the lack of the CR effect in our model. (There may be other reasons for this discrepancy, such as the effect of the short time scale dynamics. However we consider their contributions are not large compared with the CR effect.)

Nonetheless, the relaxation behavior of our model is qualitatively similar to the original model with the CR effect. To see it clearly, we show the shear relaxation moduli shifted vertically and horizontally in Figure 7(b). The data by our model (solid curves in Figure 7(a)) are shifted (the data by the original model are not shifted). For relatively long time region ( $t \gtrsim \tau_0$ ), our data can be collapsed to the data obtained by the original model well. The horizontal and vertical shift factors,  $\tilde{a}$  and  $\tilde{b}$ , are of the order of unity ( $\tilde{a} \approx 1.9$  and  $\tilde{b} \approx 0.8$  for  $N = 128$ ), and they slightly depend on  $N$ . This will be due to the difference between the dependences of relaxation mechanisms to  $N$ .

Figure 8 shows zero shear viscosities calculated by our model and the original model (with or without the CR effect). The data of the original model is taken from Fig. 5(a) of Ref 10. We can observe that for large  $N$ ,  $\eta_0$  by our model is close to the one by the original model without the CR. On the other hand, for small  $N$ , our model gives smaller  $\eta_0$  compared with the original model. We consider this is due to the difference of the dynamics of slip-springs. In our model, slip-springs can be attached only on beads while in the original model, slip-springs can be attached in between beads. Besides, our model allows slip-springs to pass through each other. The slip-spring dynamics of our model seems to give faster relaxation for small  $N$ , compared with the original model.

From the above comparisons for  $G(t)$  and  $\eta_0$ , we conclude that our model can reproduce rheological properties of the original model qualitatively well, especially for well entangled polymers. The relaxation time or the zero shear viscosity are close to the data by the original model without the CR effect. This is natural since our model does not incorporate the CR effect. Nonetheless, the relaxation behavior of our model is almost the same as one of the original model in the long time region ( $t \gtrsim 10\tau_0$ ).

## 4.3 Acceleration by GPU

In the previous subsection, we have shown that the single chain slip-spring model can reproduce rheological properties qualitatively. In this subsection we show the results of the acceleration by a GPU. To study the acceleration, we compare the calculation times on a CPU and on a GPU, by using the same parameter set. As an example, in this work we use Intel Core 2 Duo E8500 (3.16GHz, dual-core) for simulations on CPU, and NVIDIA Tesla C1060 (1.3GHz, 240 CUDA cores) for simulations on GPU. Simulation programs are written in C and CUDA for CPU and GPU, respectively. They are compiled by using gcc (version 4.3.0) and nvcc (version 2.1) and executed on Linux (kernel 2.6.9, x86\_64). The program for CPU is written in ANSI C and

no CPU-specific extensions (such as the SSE or SSE2 instruction sets [54]) are utilized. The numbers of threads used for the calculations are 1 (CPU) and  $128 \times 128$  (GPU). For comparison, we performed simulations with the following parameters; the numbers of beads and chains  $N \times M = 16 \times 4096, 32 \times 2048, 64 \times 1024$ , or  $128 \times 512$  (the total number of beads is kept to be constant), the shear rate  $\dot{\gamma} = 0$  or 0.05. All the simulations are started from the equilibrium initial state (at time  $t = 0$ ). The time step size is  $\Delta t = 0.01$ , and the simulations are stopped at time  $t = 100$  (the total number of time steps is 10000). The results are summarized in Table 1. We can observe that the program for GPU is about 290 times faster than the program for CPU. The acceleration by a GPU is quite effective to accelerate our single chain slip-spring model.

## 5 Discussion

### 5.1 Model Properties

We formulated a single chain version of the slip-spring model for entangled polymers. Our model is designed as the simplified model of the original one. One notable property of our model is that it fully satisfies the detailed balance condition. This means that the equilibrium probability distribution rigorously becomes the Boltzmann distribution. This enables us to tune the equilibrium statistics of the model easily. For example, we can employ the statistics of a non-ideal chain (real chain) for our model, or we can introduce the interaction between slip-springs. Such modifications can be done essentially only by changing the expression for the grand potential (2).

Because it is reported that the statistics of entangled polymer chains somehow depend on models (such as primitive path extraction methods [55–57] or dynamic equations [58]), it will be desirable for a model to be tunable for a specific target statistics. The equilibrium distribution function (13) has a rather simple structure and we can tune, for example, the statistics of the chain or the statistics slip-springs easily. We expect that our model can be used to investigate rheological behaviors for various chain statistics models numerically.

The detailed balance condition also becomes important when we derive the linear response formula (43). Although the response formula (43) itself is already proposed by Ramirez, Sukumaran and Likhtman [43], they did not give the derivation based on the master equation. We gave the rigorous derivation based on the master equation, which corresponds to the Langevin and jump dynamics actually used in the simulations. Our result justifies the use of the response formula (43) to calculate the relaxation modulus tensor.

Although dynamics of slip-springs is modeled as a simple jump dynamics in our model, it can reproduce linear and nonlinear rheological behaviors qualitatively. The linear rheological properties are similar to the original slip-spring model. This implies that our model captures essential nature of the original slip-spring model. We also performed simulations for nonlinear rheological properties, and reproduced the viscosity growth and the Cox-Merz rule. Thus we consider that our single chain slip-spring model can be used as long as we want to calculate simple rheological properties.

In our model, the rheological properties can be reproduced well while there is no CR effect. As we already pointed, even without the CR effect, there is a CR like relaxation mechanism in our model (as shown in Appendix A). This relaxation mechanism is caused by the model property that slip-springs can pass through (or exchange) each other. Our result implies that in some situations, this “constraint exchange” mechanism can be employed instead of the CR mechanism. From the numerical point of view, if we allow slip-spring to pass through each other, the implementation becomes much easier (this is because the time evolution of each slip-springs can be evaluated in parallel). It seems to not be difficult to make slip-springs exchangeable in other slip-link type models. The exchangeable slip-links will improve numerical accuracy efficiently.

### 5.2 Acceleration by GPU

We observed that the acceleration by a GPU can improve the simulation speed drastically. The program for GPU is about 290 times faster than the program for CPU, which seems to be quite



efficient and promising. However, it is fair to mention about the possible acceleration by some CPU-specific extensional instructions. Several CPU-specific special extensional instructions can improve the performance largely. For example, the SSE instruction handles 4 single precision floating-point operations in parallel [54]. The use of the SSE and/or SSE2 will improve the performance roughly about 10 times (for single precision floating-point number operations). Besides, currently the program for CPU is not parallelized. Because we can achieve very high parallelism for a single chain type model, the performance can be further improved by the factor 2 (for a dual-core CPU). This means, even if we tune the program for CPU extremely and parallelize it, the GPU program is still about 15 times faster than the CPU program. (We also note that we can use multiple GPUs in parallel, and it can also improve the performance.)

Although it is possible to improve the program for CPU, typically programs with such special instructions become quite complicated. The portability of the program is also decreased if we use CPU-specific instructions explicitly. As a result, the programming cost for CPU becomes much larger than one for GPU. Judging from the acceleration effects and the programming costs, we can conclude that the single chain slip-spring model simulations on a GPU are very efficient and promising for practical purposes.

Since simulations on a GPU enable us to calculate rheological properties (such as stress tensor) very efficiently, in principle we can perform CONNFESSIT or particle type multiscale simulations [13–15] with reasonable calculation costs, by combining our single chain slip-spring model and macroscale fluid models. When we perform macroscopic fluid simulations in which many mesoscopic rheological simulations are embedded (typically several thousand mesoscopic simulators are embedded in a single fluid element), the mesoscale simulations are the most time-consuming part. If we perform such multiscale simulations only on CPUs, the required calculation time is still considerable even if we parallelize the mesoscopic simulator. Our simulation model and use of a GPU can decrease the mesoscopic calculation cost drastically. We expect that the total simulation time of multiscale simulations can be also reduced drastically. Besides, the mesoscopic rheological simulations can be further accelerated by using multiple GPUs (because our simulations are already highly parallelized). Cooperating our model with macroscale fluid models will be future works.

To study rheological properties of complicated systems, such as the rheology of branched polymers or polymer blends, we will need to refine our model. We will be also required to take into account of the CR or the CCR, for precise calculations under fast shear rates. For more complex architectures, such as star polymers or comb polymers, the generalization of the model will be required. We consider that generalization itself is not so difficult, but it may be difficult to implement it for a GPU because there are several limitations for a GPU. To perform simulations efficiently on a GPU, we will need to design a generalized model so that it is suitable for calculations on a GPU.

## 6 Conclusion

In this work we proposed a single chain slip-spring model, which is based on the Likhtman’s slip-spring model [10]. The model is designed to be suitable for simulations on a GPU. Besides, the model is expressed by using the free energy and satisfies the detailed balance condition, which ensures that the system relaxes to the thermal equilibrium state. We calculated several static properties (equilibrium distribution functions) analytically. We also calculated the linear response of the system to strain deformation, and obtained the Green-Kubo type formula for the relaxation modulus which is in agreement with the one previously proposed by Ramirez, Sukumaran and Likhtman [43].

We calculated several rheological properties such as the linear viscoelasticity or the viscosity growth, and shown that our model can reproduce them reasonably. To accelerate the simulations, we performed simulations on a GPU as well as simulations on a CPU. By comparing the simulation times, we found that the use of a GPU can accelerate a simulation approximately 290 times faster. The modification of our model or the application to actual multiscale simulations will be future works.

## Acknowledgment

This work is supported by JST-CREST. The author thanks Mr. Ryuji Sakamaki for informing the author about the fixed-point real number technique and Ref 46. He also thanks to Prof. Yuichi Masubuchi for various helpful comments.

## A Constraint Release Type Relaxation Mechanism

In many models for entangled polymers, the constraint release (CR) effect is considered to be an important effect (especially for branched polymers). Several methods have been developed to take the CR events into account. Rubinstein and Colby [59] modelled the CR events as hopping motions of tube segments in a self-consistent way. Based on this idea, Schieber and coworkers [6,9,11] introduced (relatively) slow diffusion type Brownian motion of slip-links as the CR events. Masubuchi and coworkers [7] directly modelled the CR events as reconstruction of slip-links between two chains. Doi and Takimoto [8], and Likhtman [10] modelled the CR events as reconstruction events in a similar way (in their models, slip-links (slip-springs) are virtually paired). In our single chain slip-spring model, the CR process is not explicitly considered. However, as we discuss in this section, the CR type relaxation process exists (implicitly) in our model.

One peculiar property of our model is that slip-springs can pass through each other, unlike the original slip-spring model. Most of lip-link based models do not allow slip-links to pass through each other. Similarly, it is usually not allowed in most of tube models to exchange the neighboring entanglement points. Then, we can expect that the passing-through events of slip-springs will result in a sort of relaxation process.

We consider a passing-through event of two neighboring slip-springs. Here we label the slip-spring indices  $j$  in the following order (ascending in  $S_j$ ) to compare our model with conventional models.

$$S_1 \leq S_2 \leq S_3 \leq \dots \leq S_Z \quad (67)$$

This condition is (implicitly) assumed in many slip-link based models. If the  $j$ -th and  $(j + 1)$ -th slip-springs are exchanged at time  $t$ , then we should exchange the slip-spring indices and anchoring points to satisfy the condition (67).

$$S_j(t + 0) = S_{j+1}(t), \quad S_{j+1}(t + 0) = S_j(t) \quad (68)$$

$$\mathbf{A}_j(t + 0) = \mathbf{A}_{j+1}(t), \quad \mathbf{A}_{j+1}(t + 0) = \mathbf{A}_j(t) \quad (69)$$

This dynamics of two monomer indices,  $S_j$  and  $S_{j+1}$ , can be interpreted as the collision and reflection like dynamics. The dynamics of two anchoring points,  $\mathbf{A}_j$  and  $\mathbf{A}_{j+1}$ , can be interpreted as sudden jumps in space. We consider that such jump events are similar to the CR picture considered by Rubinstein and Colby [59]. Thus, we can interpret the exchange events as the CR like motions of anchoring points. Then the exchange events effectively give the CR like stress relaxation process.

However, we should notice that the exchange events do not exactly correspond to the conventional CR events. For example, our CR like events are non-Markovian while the CR events are usually modelled as Markovian. (This is because after one exchange event, the same slip-spring pair can pass through each other again. Such a process results in the memory effect.) Thus the effect of the exchange events to the stress relaxation is expected not to be strong at long time scale. To fully take account of the conventional CR events, we will need to model the CR process in our model as another jump process.

## B Detailed Calculations in Linear Response Theory

In this appendix, we show detailed calculations in the derivation of the linear response of the stress to the velocity gradient tensor. Although the calculations themselves are rather straightforward, the final result is not so intuitive. We show detailed calculations to avoid confusions. We note that,

following the same procedure, one can derive other linear response functions such as the dielectric response function. Mainly we follow the standard derivation of the linear response theory for the Fokker-Planck equation [42].

We may start from eq (35), the time evolution equation for the probability distribution function. If we decompose the probability distribution function into the equilibrium and perturbation parts,

$$P(\{\mathbf{r}_i\}, \{\mathbf{a}_j\}, \{s_j\}, z; t) = P_{\text{eq}}(\{\mathbf{r}_i\}, \{\mathbf{a}_j\}, \{s_j\}, z) + P_1(\{\mathbf{r}_i\}, \{\mathbf{a}_j\}, \{s_j\}, z; t) \quad (70)$$

the time evolution equation (35) can be approximately expressed as follows, by taking only the linear terms in the perturbation expansion.

$$\frac{\partial P_1}{\partial t} \approx \mathcal{L}_0 P_1 + \mathcal{L}_1(t) P_{\text{eq}} \quad (71)$$

where we used that the equilibrium part of the time evolution operator,  $\mathcal{L}_0$ , and the equilibrium distribution function  $P_{\text{eq}}$  satisfy the following equation.

$$\frac{\partial P_{\text{eq}}}{\partial t} = \mathcal{L}_0 P_{\text{eq}} = 0 \quad (72)$$

By integrating eq (71) we have

$$P_1(\{\mathbf{r}_i\}, \{\mathbf{a}_j\}, \{s_j\}, z; t) = \int_{-\infty}^t dt' e^{(t-t')\mathcal{L}_0} \mathcal{L}_1(t') P_{\text{eq}} \quad (73)$$

The average time-dependent stress tensor is then calculated to be

$$\begin{aligned} \boldsymbol{\sigma}(t) &= \sum_{z, \{s_i\}} \int d\{\mathbf{r}_i\} d\{\mathbf{a}_j\} \hat{\boldsymbol{\sigma}} P(\{\mathbf{r}_i\}, \{\mathbf{a}_j\}, \{s_j\}, z; t) \\ &= \sum_{z, \{s_i\}} \int d\{\mathbf{r}_i\} d\{\mathbf{a}_j\} \hat{\boldsymbol{\sigma}} \left[ P_{\text{eq}} + \int_{-\infty}^t dt' e^{(t-t')\mathcal{L}_0} \mathcal{L}_1(t') P_{\text{eq}} \right] \\ &= \boldsymbol{\sigma}_{\text{eq}} + \int_{-\infty}^t dt' \sum_{z, \{s_i\}} \int d\{\mathbf{r}_i\} d\{\mathbf{a}_j\} \hat{\boldsymbol{\sigma}} e^{(t-t')\mathcal{L}_0} \mathcal{L}_1(t') P_{\text{eq}} \end{aligned} \quad (74)$$

where  $\boldsymbol{\sigma}_{\text{eq}} \equiv \langle \hat{\boldsymbol{\sigma}} \rangle_{\text{eq}}$ . Eq (74) can be modified further by utilizing the following equation.

$$\begin{aligned} \mathcal{L}_1(t) P_{\text{eq}} &= \frac{1}{k_B T} \left[ \sum_{i=1}^N \left[ \frac{\partial \mathcal{J}}{\partial \mathbf{r}_i} \mathbf{r}_i - k_B T \mathbf{1} \right] + \sum_{j=1}^z \left[ \frac{\partial \mathcal{J}}{\partial \mathbf{a}_j} \mathbf{a}_j - k_B T \mathbf{1} \right] \right] : \boldsymbol{\kappa}(t) P_{\text{eq}} \\ &= \frac{1}{k_B T} [\hat{\boldsymbol{\sigma}} + \hat{\boldsymbol{\sigma}}^{(v)}] : \boldsymbol{\kappa}(t) P_{\text{eq}} \end{aligned} \quad (75)$$

where we defined the virtual stress tensor operator  $\hat{\boldsymbol{\sigma}}^{(v)}$  as

$$\hat{\boldsymbol{\sigma}}^{(v)} \equiv \sum_{j=1}^z \frac{3k_B T}{N_s b^2} (\mathbf{r}_{s_j} - \mathbf{a}_j)(\mathbf{r}_{s_j} - \mathbf{a}_j) - z k_B T \mathbf{1} \quad (76)$$

Finally we have the following expression for the time-dependent stress tensor, and thus we have eq (40).

$$\begin{aligned} \boldsymbol{\sigma}(t) &= \boldsymbol{\sigma}_{\text{eq}} + \frac{1}{k_B T} \int_{-\infty}^t dt' \sum_{z, \{s_i\}} \int d\{\mathbf{r}_i\} d\{\mathbf{a}_j\} \hat{\boldsymbol{\sigma}} e^{(t-t')\mathcal{L}_0} \left[ [\hat{\boldsymbol{\sigma}} + \hat{\boldsymbol{\sigma}}^{(v)}] : \boldsymbol{\kappa}(t') P_{\text{eq}} \right] \\ &= \boldsymbol{\sigma}_{\text{eq}} + \frac{1}{k_B T} \int_{-\infty}^t dt' \sum_{z, \{s_i\}} \int d\{\mathbf{r}_i\} d\{\mathbf{a}_j\} \left[ e^{(t-t')\mathcal{L}_0^\dagger} \hat{\boldsymbol{\sigma}} \right] [\hat{\boldsymbol{\sigma}} + \hat{\boldsymbol{\sigma}}^{(v)}] P_{\text{eq}} : \boldsymbol{\kappa}(t') \\ &= \boldsymbol{\sigma}_{\text{eq}} + \frac{1}{k_B T} \int_{-\infty}^t dt' \langle \hat{\boldsymbol{\sigma}}(t-t') [\hat{\boldsymbol{\sigma}} + \hat{\boldsymbol{\sigma}}^{(v)}] \rangle_{\text{eq}} : \boldsymbol{\kappa}(t') \end{aligned} \quad (77)$$

Here  $\mathcal{L}_0^\dagger$  is the adjoint operator of  $\mathcal{L}_0$ , which is defined via the following relation.

$$\sum_{z, \{s_i\}} \int d\{\mathbf{r}_i\} d\{\mathbf{a}_j\} \hat{B} \mathcal{L}_0 P_{\text{eq}} = \sum_{z, \{s_i\}} \int d\{\mathbf{r}_i\} d\{\mathbf{a}_j\} (\mathcal{L}_0^\dagger \hat{B}) P_{\text{eq}} \quad (78)$$

where  $\hat{B}$  is an arbitrary operator. We also defined the time-shifted operator of  $\hat{B}$  as follows, from the fact that  $\mathcal{L}_0^\dagger$  works as the equilibrium time evolution operator.

$$\hat{B}(t) \equiv e^{t\mathcal{L}_0^\dagger} \hat{B} \quad (79)$$

where  $\hat{B}$  is again an arbitrary operator.

We note that the detailed balance condition is essential in the preceding derivation of the linear response formula. If the model does not satisfy the detailed balance, generally the simple Green-Kubo type formulae such as eq (43) do not hold. Although we can calculate the linear responses even if the detailed balance condition is not satisfied, generally the resulting expressions do not reduce to the Green-Kubo form.

## References

- [1] Doi M, Edwards SF, “*The Theory of Polymer Dynamics*”, (1986), Oxford University Press, Oxford.
- [2] Ianniruberto G, Marrucci G, *J Rheol*, **45**, 1305 (2001).
- [3] Marrucci G, Ianniruberto G, *Phil Trans R. Soc Lond A*, **361**, 677 (2003).
- [4] Likhtman AE, Graham RS, *J Non-Newtonian Fluid Mech*, **114**, 1 (2003).
- [5] Kremer K, Grest GS, *J Chem Phys*, **92**, 5057 (1990).
- [6] Hua CC, Schieber JD, *J Chem Phys*, **109**, 10018 (1998).
- [7] Masubuchi Y, Takimoto J, Koyama K, Ianniruberto G, Greco F, Marrucci G, *J Chem Phys*, **115**, 4387 (2001).
- [8] Doi M, Takimoto J, *Phil Trans R Soc Lond A*, **361**, 641 (2003).
- [9] Schieber JD, Neergaard J, Gupta S, *J Rheol*, **47**, 213 (2003).
- [10] Likhtman AE, *Macromolecules*, **38**, 6128 (2005).
- [11] Nair DM, Schieber JD, *Macromolecules*, **39**, 3386 (2006).
- [12] Kindt P, Briels WJ, *J Chem Phys*, **127**, 124901 (2007).
- [13] Laso M, Öttinger HC, *J Non-Newtonian Fluid Mech*, **47**, 1 (1993).
- [14] Halin P, Lielens G, Keunings R, Legat V, *J Non-Newtonian Fluid Mech*, **79**, 387 (1988).
- [15] Murashima T, Taniguchi T, *J Polym Sci B: Polym Phys*, **48**, 886 (2010).
- [16] Yasuda S, Yamamoto R, *Europhys Lett*, **86**, 18002 (2009).
- [17] Yasuda S, Yamamoto R, *Phys Rev E*, **81**, 036308 (2010).
- [18] <http://www.peta.co.jp/>.
- [19] Susukita R, Ebisuzaki T, Elmegreen BG, Furusawa H, Kato K, Kawai A, Kobayashi Y, Koishi T, McNiven GD, Narumi T, Yasuoka K, *Comp Phys Comm*, **155**, 115 (2003).

- [20] Narumi T, Ohno Y, Futatsugi N, Okimoto N, Suenaga A, Yanai R, Taiji M, in “*Proceedings of NIC Workshop 2006, From Computational Biophysics to Systems Biology*”, *NIC Series*, **34**, 29 (2006).
- [21] <http://www.clearspeed.com/>.
- [22] “*ClearSpeed Software Development Kit Reference Manual Version 3.0*”, (2008), ClearSpeed.
- [23] <http://cell.scei.co.jp/>.
- [24] <http://www.ibm.com/developerworks/power/cell/>.
- [25] “*Cell Broadband Engine Programming Handbook Version 1.11*”, (2008), IBM.
- [26] [http://www.nvidia.com/object/cuda\\_home\\_new.html](http://www.nvidia.com/object/cuda_home_new.html).
- [27] Lindholm E, Nickolls J, Oberman S, Montrym J, *IEEE Micro*, **28**, 39 (2008).
- [28] “*NVIDIA CUDA Programming Guide Version 2.1*”, (2008), NVIDIA.
- [29] <http://ati.amd.com/technology/streamcomputing/>.
- [30] “*ATI Stream Computing User Guide rev 1.4.0a*”, (2009), AMD.
- [31] Owens JD, Luebke D, Govindaraju N, Harris M, Krüger J, Lefohn AE, Purcell TJ, *Comp Graph Forum*, **26**, 80 (2007).
- [32] Hamada T, Iitaka T, arXiv:astro-ph/0703100.
- [33] Anderson JA, Lorenz CD, Travesset A, *J Comp Phys*, **227**, 5342 (2008).
- [34] Cohen J, Garland M, *Comput Sci Eng*, **11**, 58 (2009).
- [35] Preis T, Virnau P, Paul W, Schneider JJ, *J Comp Phys*, **228**, 4468 (2009).
- [36] Januszewski M, Kostur M, *Comp Phys Comm*, **181**, 183 (2010).
- [37] Schieber JD, *J Chem Phys*, **118**, 5162 (2003).
- [38] Masubuchi Y, Ianniruberto G, Greco F, Marrucci G, *J Chem Phys*, **119**, 6925 (2003).
- [39] van Kampen NG, “*Stochastic Processes in Physics and Chemistry*”, 3rd ed, (2007), Elsevier, Amsterdam.
- [40] Glauber RJ, *J Math Phys*, **4**, 294 (1963).
- [41] Evans DJ, Morris GP, “*Statistical Mechanics of Nonequilibrium Liquids*”, 2nd ed, (2008), Cambridge University Press, Cambridge.
- [42] Risken H, “*The Fokker-Planck Equation*”, 2nd ed. (1989), Springer, Berlin.
- [43] Ramirez J, Sukumaran SK, Likhtman AE, *J Chem Phys*, **126**, 244904 (2007).
- [44] Honeycutt RL, *Phys Rev A*, **45**, 600 (1992).
- [45] Harris M, “*Optimizing Parallel Reduction in CUDA*”, in NVIDIA CUDA SDK.
- [46] Narumi T, Sakamaki R, Kameoka S, Yasuoka K, in “*Proceedings of Ninth International Conference on Parallel and Distributed Computing, Applications and Technologies (PDCAT 2008)*”, 143 (2008).
- [47] Masubuchi Y, Ianniruberto G, Greco F, Marrucci G, *J Non-Newtonian Fluid Mech*, **149**, 87 (2008).

- [48] Strobl G, “*The Physics of Polymers*”, 2nd ed., (1997), Springer, Berlin.
- [49] Fetters LJ, Lohse DJ, Colby RH, in “*Physical Properties of Polymers Handbook*”, Mark JE, ed, 2nd ed., 445 (2007), Springer, New York,
- [50] Graessley WW, “*Polymeric Liquids and Networks: Dynamics and Rheology*”, (2008), Taylor and Francis, New York.
- [51] Cates ME, McLeish TCB, Marrucci G, *Europhys. Lett.*, **21**, 451 (1993).
- [52] Mead DW, Larson RG, Doi M, *Macromolecules*, **31**, 7895 (1998).
- [53] Graham RS, Likhtman AE, McLeish TCB, Milner ST, *J. Rheol.*, **47**, 1171 (2003).
- [54] “*Intel 64 and IA-32 Architectures Software Developer’s Manual Volume 1: Basic Architecture*”, (2009), Intel.
- [55] Everaers R, Sukumaran SK, Grest GS, Svaneborg C, Sivasubramanian A, Kremer K, *Science*, **303**, 823 (2004).
- [56] Kröger M, *Comp Phys Comm*, **168**, 209 (2005).
- [57] Tzoumanekas C, Theodorou DN, *Macromolecules*, **39**, 4592 (2006).
- [58] Masubuchi Y, Uneyama T, Watanabe H, Ianniruberto G, Greco F, Marrucci G, *J Chem Phys*, **132**, 134902 (2010).
- [59] Rubinstein M, Colby RH, *J Chem Phys*, **89**, 5291 (1988).

## Figure and Table Captions

Figure 1: Storage and loss moduli calculated by the single chain slip-spring model. Circles and crosses indicate  $G'(\omega)$  and  $G''(\omega)$  calculated by simulations.

Figure 2: The longest relaxation time calculated from the linear viscoelasticity data. Broken lines show slopes 2, 3 and 3.48, which correspond to the Rouse type relaxation, the pure reptation type relaxation, and the exponent obtained by the fitting, respectively.

Figure 3: Zero shear viscosity calculated from the linear viscoelasticity data. Broken lines show slopes 1 and 3.4. The critical bead number is estimated to be  $N_c = 14.2$ . (The arrow indicates the critical bead number.)

Figure 4: Viscosity growth curves with various shear rates for  $N = 40$ . The shear rates are  $\dot{\gamma}\tau_0 = 0.0025, 0.005, 0.01, 0.025, 0.05, \text{ and } 0.1$ . The broken line shows the zero shear viscosity calculated from the linear viscoelasticity data.

Figure 5: Dynamic and steady viscosities,  $\eta^*(\omega)$  and  $\eta(\dot{\gamma})$ . Circles indicate  $\eta^*(\omega)$  and the crosses (with curves) indicate the  $\eta(\dot{\gamma})$ .

Figure 6: Relative contribution of the virtual stress to the shear relaxation modulus.

Figure 7: (a) Comparison of shear relaxation moduli calculated by original and our slip-spring models. Solid curves are calculated by our model. Dotted curves are the data of the original slip-spring model with or without the CR effect (taken from Fig. 4(a) of Ref 10).  $N = 8, 16, 32, 64$  and 128, from left to right. (b) The same data with (a) but data calculated by our model are shifted horizontally and vertically.

Figure 8: Comparison of zero shear viscosities calculated by original and our slip-spring models. Circles are calculated by our model (and the same as the data shown in Figure 3). Crosses and triangles are the data of the original slip-spring model with and without CR (taken from Fig. 5(a) of Ref 10).

Table 1: Calculation times with various simulation parameters on a CPU and on a GPU.  $N, M, \dot{\gamma}$  are the number of beads per chain (polymerization index), the total number of chains, and the shear rate.  $t_{\text{CPU}}$  and  $t_{\text{GPU}}$  are the calculation times on a CPU (Intel Core 2 Duo E8500, single thread) and on a GPU (NVIDIA Tesla C1060,  $128 \times 128$  threads), respectively. Simulations are performed from  $t = 0$  (in equilibrium) to  $t = 100$  with the time step size  $\Delta t = 0.01$ . The speed-up factor is defined as the ratio of calculation times,  $t_{\text{CPU}}/t_{\text{GPU}}$ .

# Figures

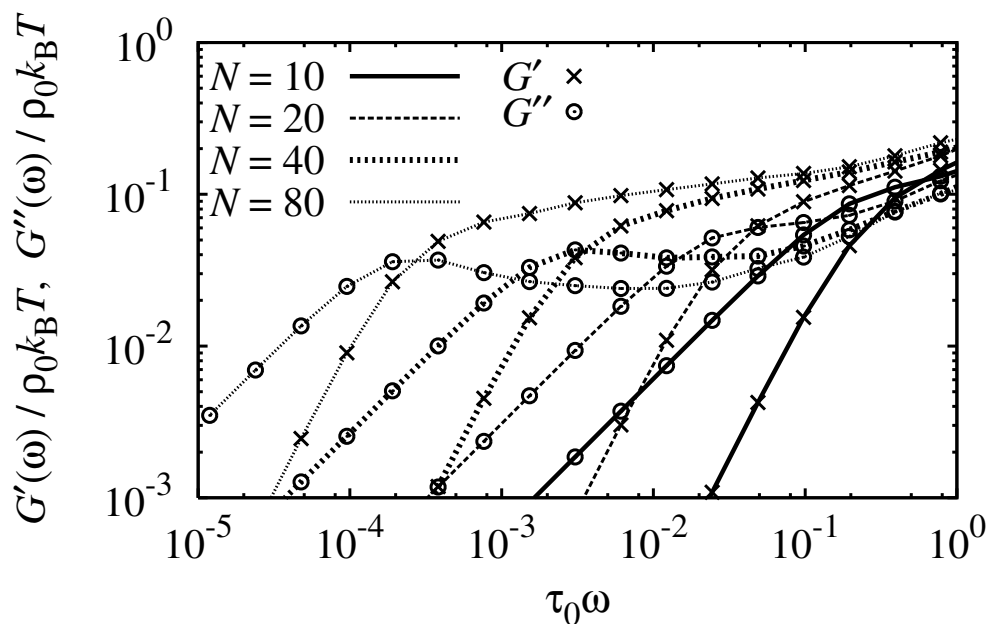


Figure 1:



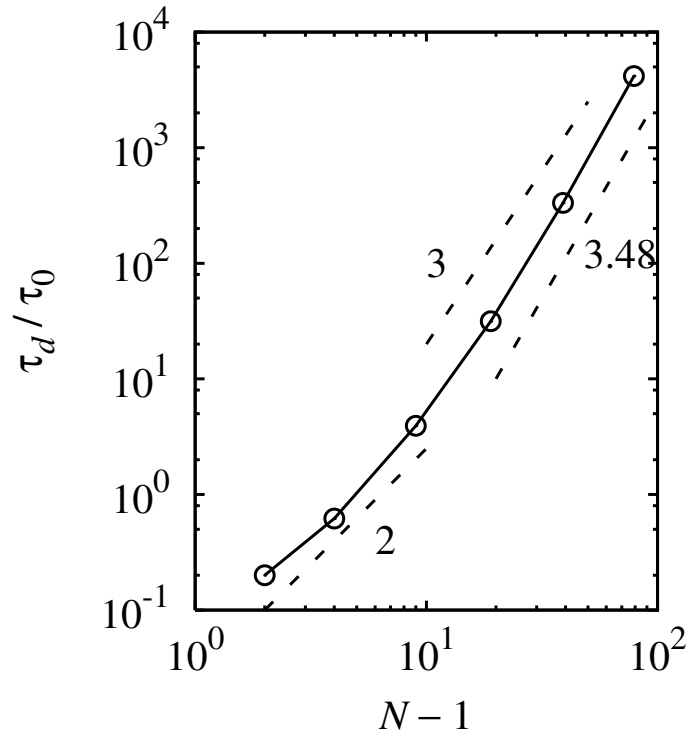


Figure 2:

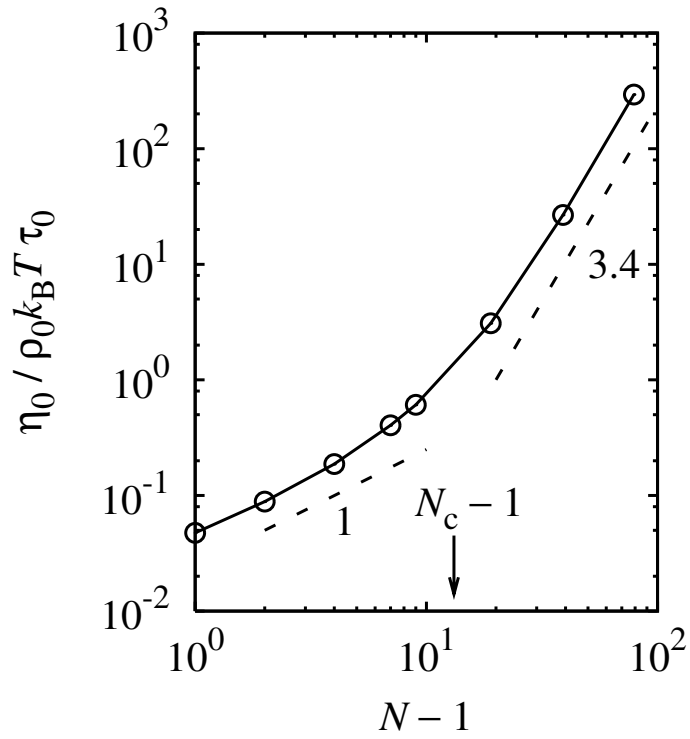


Figure 3:

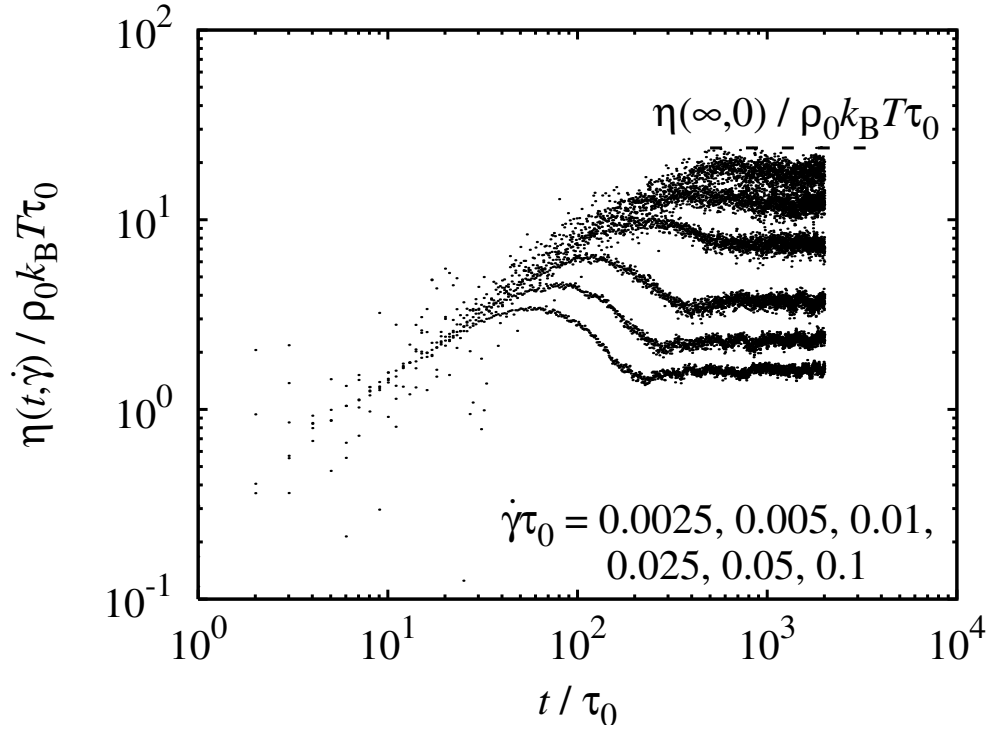


Figure 4:

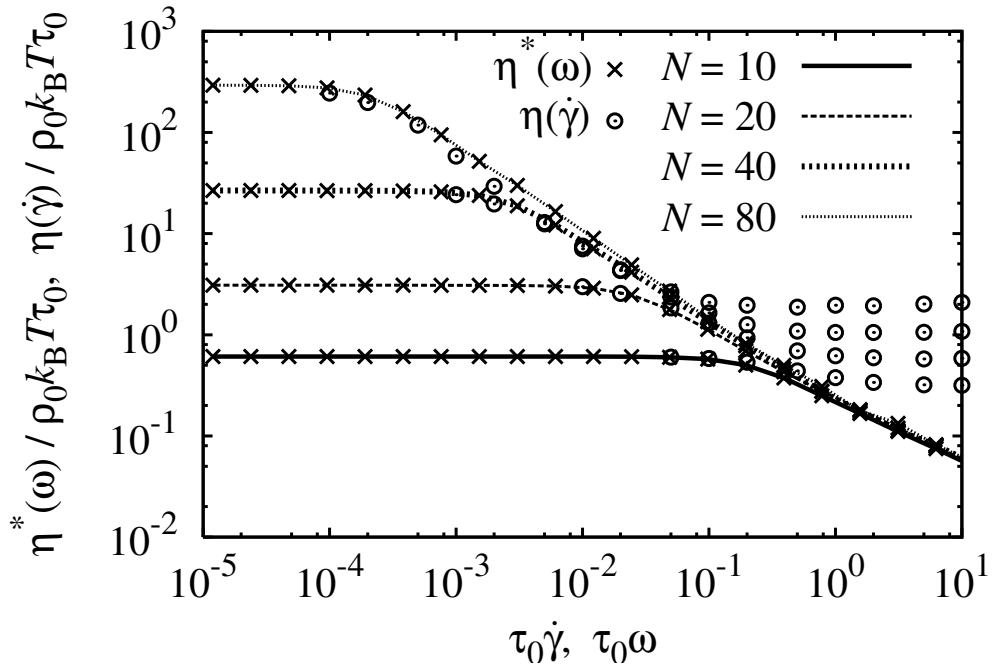


Figure 5:

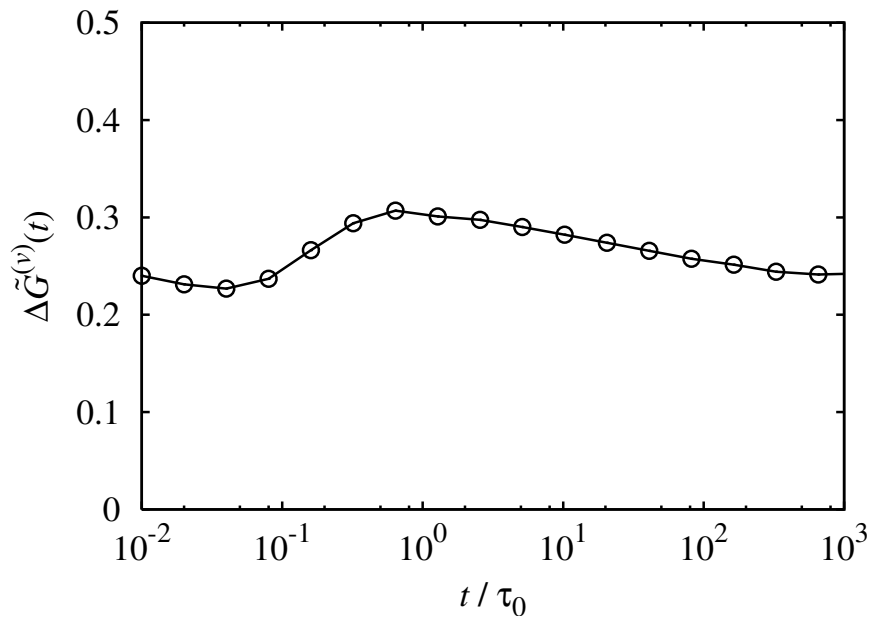


Figure 6:

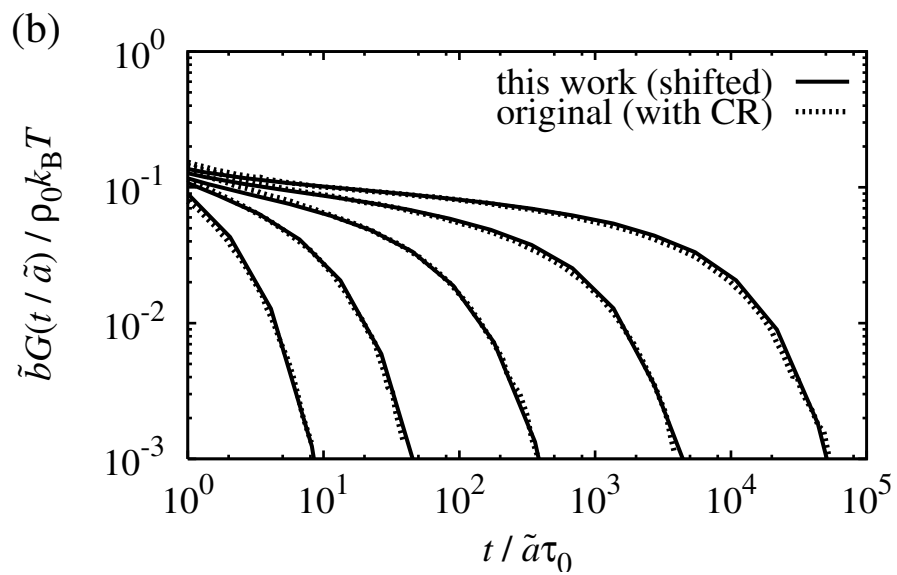
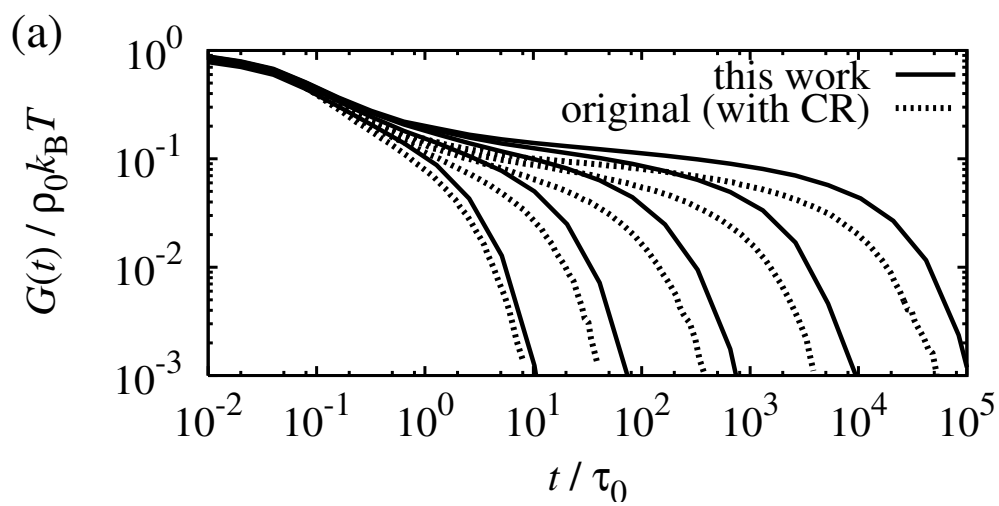


Figure 7:

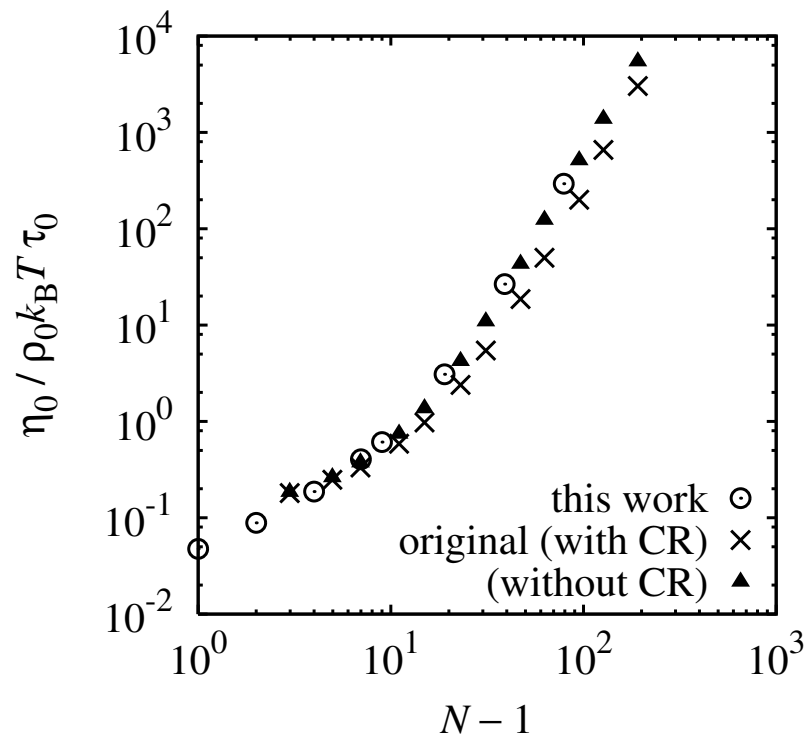


Figure 8:

## Table

$N \times M$	$\dot{\gamma}$	$t_{\text{CPU}}[\text{s}]$	$t_{\text{GPU}}[\text{s}]$	speed-up
$16 \times 4096$	0	$2.66 \times 10^2$	$8.97 \times 10^{-1}$	297
$16 \times 4096$	0.05	$2.65 \times 10^2$	$8.95 \times 10^{-1}$	296
$32 \times 2048$	0	$2.58 \times 10^2$	$9.02 \times 10^{-1}$	286
$32 \times 2048$	0.05	$2.57 \times 10^2$	$8.95 \times 10^{-1}$	287
$64 \times 1024$	0	$2.52 \times 10^2$	$8.70 \times 10^{-1}$	291
$64 \times 1024$	0.05	$2.51 \times 10^2$	$8.63 \times 10^{-1}$	292
$128 \times 512$	0	$2.51 \times 10^2$	$8.45 \times 10^{-1}$	297
$128 \times 512$	0.05	$2.50 \times 10^2$	$8.40 \times 10^{-1}$	298

Table 1: